The nature of the interface between basalts and serpentinized mantle in oceanic domains: Insights from a geological section in the Alps

Rémi Coltat, Yannick Branquet, Pierre Gautier, Philippe Boulvais, Gianreto Manatschal

Journal Pre-proof

The nature of the interface between basalts and serpentinized mantle in oceanic domains: Insights from a geological section in the Alps

Rémi Coltat, Yannick Branquet, Pierre Gautier, Philippe Boulvais, Gianreto Manatschal

Please cite this article as: R. Coltat, Y. Branquet, P. Gautier, et al., The nature of the interface between basalts and serpentinized mantle in oceanic domains: Insights from a geological section in the Alps, *Tectonophysics* (2020), https://doi.org/10.1016/j.tecto.2020.228646

The nature of the interface between basalts and serpentinized mantle in oceanic domains: insights from a geological section in the Alps

Rémi Coltat[1], Yannick Branquet[1, 2], Pierre Gautier[1], Philippe Boulvais[1], Gianreto Manatschal[3]

[1]Univ Rennes, CNRS, Géosciences Rennes – UMR 6118, F-35000 Rennes, France

[2]Institut des Sciences de la Terre d'Orléans, UMR 7327, Université d'Orléans, Orléans, France

[3]Institut de Physique du Globe de Strasbourg, EOST-CNRS UMR 7516, Université de Strasbourg, Strasbourg France

Corresponding author: Rémi Coltat, Univ Rennes, CNRS, Géosciences Rennes – UMR 6118, F-35000 Rennes, France. remi.coltat@univ-rennes1.fr

HIGHLIGHTS

- Deformation at the basalt-serpentinite interface occurred under oceanic extension
- The interface acted as a decoupling level with bulk co-axial deformation
- The contact was not reactivated during Alpine overprint
- Fluid-assisted deformation led to carbonation of the basalts and serpentinites
- A third type of oceanic basalt-serpentinite interface is defined

ABSTRACT

The association of mafic extrusive rocks and serpentinized mantle rocks is a common feature encountered in numerous ultra-distal magma-poor rifted margins as well as in (ultra)slow-spreading oceanic settings where detachment faulting and mantle exhumation occur. Although seismic imaging and high-resolution TOBI radar allow imaging this association, the nature of this interface is poorly understood (e.g. nonconformity vs. tectonic channelized vs. diffuse fluid flow along the interface). The timing between magmatism and active detachment faulting is often poorly constrained and it remains difficult to decipher if mafic extrusives are pre-, syn- or post-exhumation of mantle rocks at the seafloor. In this study, we characterize the nature of this interface from a section of a Jurassic ultra-distal margin preserved in the

Platta nappe, SE Swiss Alps. We show that the basalt-serpentinized mantle contact does neither correspond to an Alpine thrust system, nor to a nonconformity or a detachment plane exhuming mantle rocks from underneath already emplaced basalts. Rather, the basalt-serpentinite interface corresponds to a weak decoupling level formed by conjugate low-angle normal faults onto which conjugate high-angle normal faults branch. These structures are diagnostic of co-axial extensional tectonics occurring during and after emplacement of basalts over a formerly exhumed serpentinized mantle. Carbonate extensional and shear veins and foliated ophicalcites formed during this Jurassic extensional event. Their distribution across and along the basalt-serpentinite interface demonstrates that this decoupling interface was a high-permeability layer that channelized high fluid flow responsible for the widespread hydrothermal alteration. A positive feedback between fluid flow and extensional deformation is proposed.

Keywords: extensional tectonics, basalt-serpentinite interface, ultra-distal magma-poor rifted margin, fluid-assisted deformation, ophicalcites, Alpine ophiolites

1. INTRODUCTION

Mafic extrusive rocks (e.g. basaltic lava flows, pillow basalts, hyaloclastites) overlying serpentinized mantle are a common feature of oceanic domains where serpentinized mantle rocks are exhumed to the seafloor, either in oceanic areas formed at slow- to ultraslow-spreading Mid-Oceanic Ridges (MORs) or in the ultra-distal part of "magma-poor" continental rifted margins. In present-day oceans and margins, the roughly flat-lying (i.e., subhorizontal to shallow-dipping) interface between mafic extrusives and serpentinized mantle rocks is imaged by geophysical data (Canales et al., 2004; Hopper et al., 2004; Welford et al., 2010; Sauter et al., 2013; Gillard et al., 2017) (fig. 1a-c), but its nature is poorly constrained.

In the literature, two contrasting interpretations can be found for this interface (e.g., Lagabrielle et al., 2015). The first interpretation considers it as equivalent to a nonconformity, that is, the contact represents a paleo-seafloor surface exposing ultramafic rocks, over which the volcanic material spreads (e.g., Lagabrielle and Cannat, 1990) (fig. 1d). In this case, volcanic activity postdates the exhumation of the mantle rocks to the seafloor. The second interpretation stems from the identification of shallow-dipping extensional detachments at the ultra-distal part of magma-poor rifted margins (e.g., Boillot et al., 1987, 1995) and at slow-spreading MORs (e.g., Karson and Winters, 1992; Cann et al., 1997; Tucholke et al., 1998).

In this context, a roughly flat interface between mafic extrusives and serpentinized mantle rocks may correspond to the detachment itself, the extrusives being part of the hangingwall block, possibly forming isolated extensional allochthons (or "rider blocks", or "rafts"; e.g., Karson and Winters, 1992; Cann et al., 1997; Karson et al., 2006) (fig. 1e). In this case, the contact is tectonic and volcanic activity, while possibly coeval with early stages of mantle exhumation, precedes the time at which the serpentinized mantle rocks reach the seafloor.

The two types of interpretation are illustrated by the case shown in figure 1c, where 'A-type' patches are interpreted as volcanic material spread over serpentinized mantle rocks exhumed in the footwall of an early detachment (i.e., the hypothesis of a nonconformable contact) whereas the 'B-type' patch is interpreted as a raft block in the hangingwall of a younger detachment with opposite dip (i.e., the hypothesis of a tectonic contact) (Sauter et al., 2013). Nevertheless, until now, no oceanic detachment with mafic extrusives in its hangingwall has been directly accessed and sampled. For instance, attempts to drill through such a presumed detachment, on the flank of the Atlantic Massif oceanic core complex (OCC) failed (Blackman et al., 2011).

Many studies onland (mostly in the Alpine realm) have also focused on geological sections thought to expose more or less preserved examples of a slow-spreading MOR and/or magma-poor ultra-distal margins. In these studies, when mafic extrusives overlie serpentinized mantle rocks, the contact is always interpreted as a nonconformity (e.g., Tricart and Lemoine, 1983; Lagabrielle and Cannat, 1990; Principi et al., 2004), even in cases where the existence of a major pre-orogenic extensional detachment is also suspected or established (e.g., Lemoine et al., 1987; Desmurs et al., 2001; Manatschal et al., 2011; Lagabrielle et al., 2015; Decarlis et al., 2015). The reason for this interpretation is the local but common occurrence, at the base of the extrusive sequence, of sedimentary breccias containing clasts of the underlying serpentinites (fig. 1d). Noticeably, the same interpretation is given in the case of the Platta nappe, in the Central Alps, where the geological section of this study lies (Manatschal and Nievergelt, 1997; Desmurs et al., 2001; Epin et al., 2017, 2019; Ribes et al. 2019). Due to this relation implying volcanic activity after mantle exhumation, and because gabbro bodies hosted by the serpentinized mantle rocks occasionally show evidence of syn-emplacement deformation, the hypothesis of distinct episodes of mafic magmatism (syn- vs. post-mantle exhumation) has emerged (e.g., Lemoine et al., 1987; Desmurs et al., 2001, Epin et al. 2019). In present-day oceans, basaltic cones or patches overlying serpentinized mantle rocks exhumed by a detachment are sometimes interpreted as being emplaced after

exhumation (e.g., Tucholke et al., 2001; Sauter et al., 2013) ('A-type' patches in fig. 1c). Together with other observations, these features have led to a concept whereby extension in magma-poor oceanic environments may proceed through alternated periods of localized detachment-type faulting associated with the emplacement and progressive exhumation of gabbro bodies, and more distributed high-angle faulting associated with the emplacement of dykes and volcanic material (Tucholke et al., 2001; Ildefonse et al., 2007; MacLeod et al., 2009; Manatschal et al., 2011; Lagabrielle et al., 2015; Gillard et al., 2016b). In this frame, mafic extrusives non-conformably overlying serpentinized mantle do postdate an episode of mantle exhumation but are not necessarily post-tectonic. Instead, they may represent syn-tectonic deposits emplaced during a later episode of high-angle normal faulting, the faults being used as pathways for the ascending magmas (Manatschal et al., 2011; Decarlis et al., 2018; Epin et al., 2019; Ribes et al., 2019) (fig. 1f). Such relatively late mafic extrusives are thus expected to show two types of relation with serpentinized mantle rocks, (i) a nonconformity, where the contact is roughly flat-lying, or (ii) a fault where the contact is steeply or moderately dipping. This dual relationship seems frequent in oceanic domains (e.g., Lagabrielle et al., 1998; Manatschal et al., 2011; Decarlis et al., 2018; Epin et al., 2019).

Despite the syn-tectonic nature of the late mafic extrusives, the common view is that, where their contact with the serpentinized mantle rocks is a nonconformity, they seal the contact and no significant deformation occurred along this interface during and after their emplacement (at least until the subsequent orogeny, in the case of ophiolites emplaced in orogens). In addition, the rock sequence underneath the mafic extrusives commonly shows evidence of pervasive carbonation, forming ophicalcites, which attest for important fluid circulations. Two types of ophicalcites are usually distinguished ('OC1' and 'OC2', Lemoine et al., 1987). OC1 represent tectonic(-hydraulic) breccias formed at the expense of the ultramafic rocks while OC2, overlying OC1, represent sedimentary breccias that mark the base of the nonconformable sequence (e.g., Tricart and Lemoine, 1983; Ribes et al., 2019). Ophicalcites attest for interactions between ultramafic rocks and seawater (as does serpentinization, which usually occurs before carbonation) and are classically considered to be developed at the seafloor or very close to it (e.g., Bonatti et al., 1974; Bernoulli and Weissert, 1985; Lemoine et al., 1987; Treves and Harper, 1994; Picazo et al., 2013). As a result, when ophicalcites occur at the base of a nonconformable sequence that includes mafic extrusives, carbonation is thought to predate the emplacement of the extrusives and to be related to the earlier episode of mantle exhumation (e.g., Lemoine et al., 1987; Desmurs et al.,

2001; Ribes et al., 2019; Epin et al., 2019). Therefore, the above statement may be extended as follows: in oceanic domains, when mafic extrusives overlie serpentinized mantle rocks through a flat-lying nonconformity, the common view is that neither significant deformation nor pervasive fluid circulation occurred along this interface during and after the emplacement of the extrusives.

In contrast with this view, Coltat et al. (2019a) recently argued that carbonation along such an interface can develop syn-kinematically in the aftermath of the emplacement of the extrusive rocks, at temperatures around 100ºC. Hence, it appears that a nonconformable interface between mafic extrusives and serpentinized mantle rocks is not always a static contact since significant deformation and fluid circulation may occur along it during oceanic extension

In this study, we describe a 350 m-long geological section that encompasses the outcrop studied by Coltat et al. (2019a). The distribution of deformation and the interactions between fluids, rocks, and deformation are described in detail, which allows to document how the interface between mafic extrusives and serpentinized mantle rocks behaved during and after the emplacement of the volcanic series. At the scale of the section, a pattern of symmetrical extension is observed, which contrasts with the pattern that would be expected from the development of a large extensional detachment. We discuss the tectonic setting that could have led to this situation and infer that mechanical weakening due to fluid-rock interactions is the process that allowed the previous nonconformable interface to become a decoupling level along which strain localized (i.e. a sort of décollement, though without a steady sense of shear). Thus, this study leads to the identification of a third type of interface between mafic extrusives and serpentinized mantle rocks in oceanic domains, which is neither a static nonconformity nor an extensional detachment, but a nonconformity reactivated as a decoupling level.

Figure 1. a) to c) Present-day oceanic domains showing the direct superposition of mafic extrusive rocks onto serpentinized mantle rocks, either in the ultra-distal part of a magma-poor continental margin (a, b) or at ultraslow-spreading mid-oceanic ridge (c). On (c), A and B areas correspond to volcanic eruptions on the exhumed detachment surface and rafted blocks, respectively. a, b, and c adapted from Hopper et al. (2004), Gillard et al. (2017), and Sauter et al. (2013), respectively. d) to f) Sketches illustrating the different interpretations found in the literature for the interface between mafic extrusives and serpentinized mantle rocks. d, e, and f adapted from Lagabrielle and Cannat (1990), Karson et al. (2006), and Manatschal et al. (2011), respectively.

2. GEOLOGICAL SETTING

2.1. The Platta nappe

The Platta nappe is located in southeastern Switzerland, within the Central Alps, and is part of the Piemonte-Liguria units that show an oceanic affinity (fig. 2a). The Platta nappe belongs to

the Upper Penninic nappe system, which underlies the Lower Austroalpine nappes, the latter exposing remnants of the distal margin of the Adriatic continent (e.g., Trümpy, 1975; Mohn et al., 2011). The dominant lithologies in the Platta nappe are serpentinized peridotites and basalts (massive lava flows, pillow basalts and hyaloclastites, Dietrich, 1969), together with minor gabbro bodies. Two main structural units are distinguished (Desmurs et al., 2001, 2002). The Upper Platta unit, almost entirely made of serpentinites, is restricted to the eastern part of the nappe (fig. 2b) and correlates further north and south with two other Upper Penninic nappes, the Totalp unit and Malenco nappe (e.g., Müntener et al., 2010). In the Lower Platta unit, mafic magmatism is more widespread (fig. 2b). This rock association may correspond to either an oceanic seafloor formed at a slow-spreading MOR or/and the most distal part of a magma-poor continental margin (Epin et al. 2019). The Platta nappe is separated from the continental lithologies of the overlying Err unit (one of the Lower Austroalpine nappes) by an Alpine thrust, which accommodated an unknown amount of shortening. Therefore, in principle, the lower Platta unit may have formed as an oceanic seafloor at some distance from the margin (Epin et al. 2019). However, its initial proximity with the margin is testified by two features. Firstly, the unit includes a few slivers of continental material (in purple in fig. 2b) that were incorporated in the "oceanic" rock assemblage before the Alpine orogeny (Froitzheim and Manatschal, 1996; Manatschal and Nievergelt, 1997; Epin et al., 2017, 2019). Secondly, as for the bulk of the Piemonte-Liguria units, the geochemical characteristics of the ultramafic rocks are not those of a typical oceanic lithosphere (Müntener et al., 2010; Picazo et al., 2016). The Upper and Lower Platta units rather correspond to a preserved subcontinental mantle and a refertilized (through the infiltration of asthenospheric melts) subcontinental mantle, respectively (Müntener et al., 2010).

In spite of the Alpine orogenic overprint, several extensional detachments dating from the establishment of the continental margin of Adria in the Jurassic have been identified in the Lower and Middle Austroalpine nappes situated east of the Platta nappe (Froitzheim and Eberli, 1990; Froitzheim and Manatschal, 1996; Manatschal and Nievergelt, 1997; Mohn et al., 2011, 2012; Epin and Manatschal, 2018). All these detachments display top-to-the-west kinematics. In the Platta nappe, an additional west-dipping extensional detachment dating from the late stages of rifting was recently reported (Epin et al., 2019). By analogy with observations made in Piemonte-Liguria units located further to the northeast (Tasna and Totalp; Manatschal et al., 2006; Picazo et al., 2013), this large detachment within the Platta

nappe is tracked through the local occurrence of zones of high strain showing a vertical distribution of fault rocks (from serpentinite cataclasites to serpentine gouges) that suggests a progressive exhumation of the mantle rocks during deformation (Epin et al., 2017, 2019). The fault sequence is locally capped by sedimentary breccias containing clasts of the fault rocks while the breccias themselves are overlain by basaltic flows or pelagic sediments, which supports the fault zone being related to rifting (Epin et al., 2017, 2019; Ribes et al., 2019). Furthermore, the ubiquitous development of ophicalcites at the top of the fault sequence is interpreted as marking the ultimate exposure of the detachment at the seafloor, before deposition of the volcano-sedimentary series (see also Lemoine et al., 1987; Picazo et al., 2013). However, in at least one case in the Platta nappe, pervasive carbonation demonstrably occurred at depth after the emplacement of the extrusive rocks (Coltat et al., 2019a), showing that caution is required before including ophicalcites in the typical rock sequence of detachments that exhume the mantle.

Time constraints for the episode of rifting in the Platta nappe are provided by (i) the age of mafic intrusions (among which gabbros that show evidence of syn-kinematic emplacement, Desmurs et al., 2001) dated at ~160 Ma (U-Pb zircon ages, Schaltegger et al., 2002), and (ii) Late Jurassic radiolarites and latest Jurassic-Early Cretaceous limestones and shales that form a homogeneous post-rift blanket across the paleomargin (Dietrich, 1970; Weissert and Bernoulli, 1985; Manatschal and Nievergelt, 1997; Epin et al., 2017; Ribes et al., 2019).

In the Platta nappe and adjacent Lower Austroalpine nappes, the Alpine orogeny involved several deformation phases (e.g., Froitzheim et al., 1994; Handy, 1996; Handy et al., 1996; Manatschal and Nievergelt, 1997; Mohn et al., 2011). The first phase, named the Trupchun or D1 phase of Late Cretaceous age, is considered to have produced the main structures within the Platta nappe and at its eastern contact with the Err nappe (Manatschal and Nievergelt, 1997; Epin et al., 2017). These structures consist of shallow-east-dipping thrusts with a top-to-the-west, or locally top-to-the-northwest, sense of shear. Hence, Late Cretaceous thrusts and the extensional detachments associated with Jurassic rifting had similar kinematics, making their distinction in the field difficult if only kinematic data is used.

The second phase of deformation, named the Ducan-Ela or D2 phase of latest Cretaceous age, was identified in the Austroalpine nappes located northeast and southeast of the Platta nappe (Froitzheim et al., 1994; Handy, 1996). It produced large recumbent folds and low-dipping normal faults with a top-to-the-east to southeast sense of shear, reactivating

D1 thrusts. In contrast, the impact of D2 within the Platta nappe seems limited. At the northeastern margin of the nappe, east of the site of this study, the "Piz d'Err frontal fold", a kilometer-scale north-facing anticline that was attributed to the D2 phase (Froitzheim et al., 1994; Manatschal and Nievergelt, 1997) is now interpreted as resulting from the D3 compressional phase (see below; Epin and Manatschal, 2018). Top-to-the-east ductile shear fabrics within gabbros located east of the Marmorera Lake were used to infer the existence of a D2 extensional shear zone cutting down into the Platta nappe (Manatschal, 1995; Manatschal and Nievergelt, 1997). However, as discussed by Desmurs et al. (2001), this deformation is far more likely to be related to Jurassic rifting.

The third phase of deformation, named the Blaisun or D3 phase, occurred during the Cenozoic and resulted from renewed orogenic shortening in a north-south direction. It produced east-west-trending folds with steeply-dipping axial planes and a few north-vergent thrusts (Froitzheim et al., 1994; Epin et al., 2017).

Alpine metamorphism had a variable imprint across the Platta nappe, with higher grade conditions prevailing in the south (e.g., Dietrich, 1969; Dietrich et al., 1974; Mohn et al., 2011). In the northern part of the nappe, where the site of this study lies, Alpine metamorphism occurred at temperatures of ~300-325ºC as inferred from the mineralogical record in the Late Jurassic-Early Cretaceous post-rift sediments (Ferreiro Mählmann, 1995, 2001). In line with these findings, the mafic extrusive rocks show typical pumpellyite-bearing assemblages (Dietrich, 1969; Dietrich et al., 1974). In this low-grade northern part of the nappe, syn-kinematic greenschist facies (albite-epidote-chlorite) assemblages are also found at the base of some of the extrusive bodies, within deformed basalts that overlie serpentinites, like at the Marmorera outcrop (Epin et al., 2019) and on the site of this study (Coltat et al., 2019b) (Fig. 2b). Together with other arguments, this spatial coincidence pleads for the development of such assemblages as a result of hydrothermal alteration during the rifting episode (Epin et al., 2019; Coltat et al., 2019a, b, see also this work). Similarly, some gabbros display a progressive evolution from syn-magmatic to greenschist facies deformation that must relate to rifting (Desmurs et al., 2001).
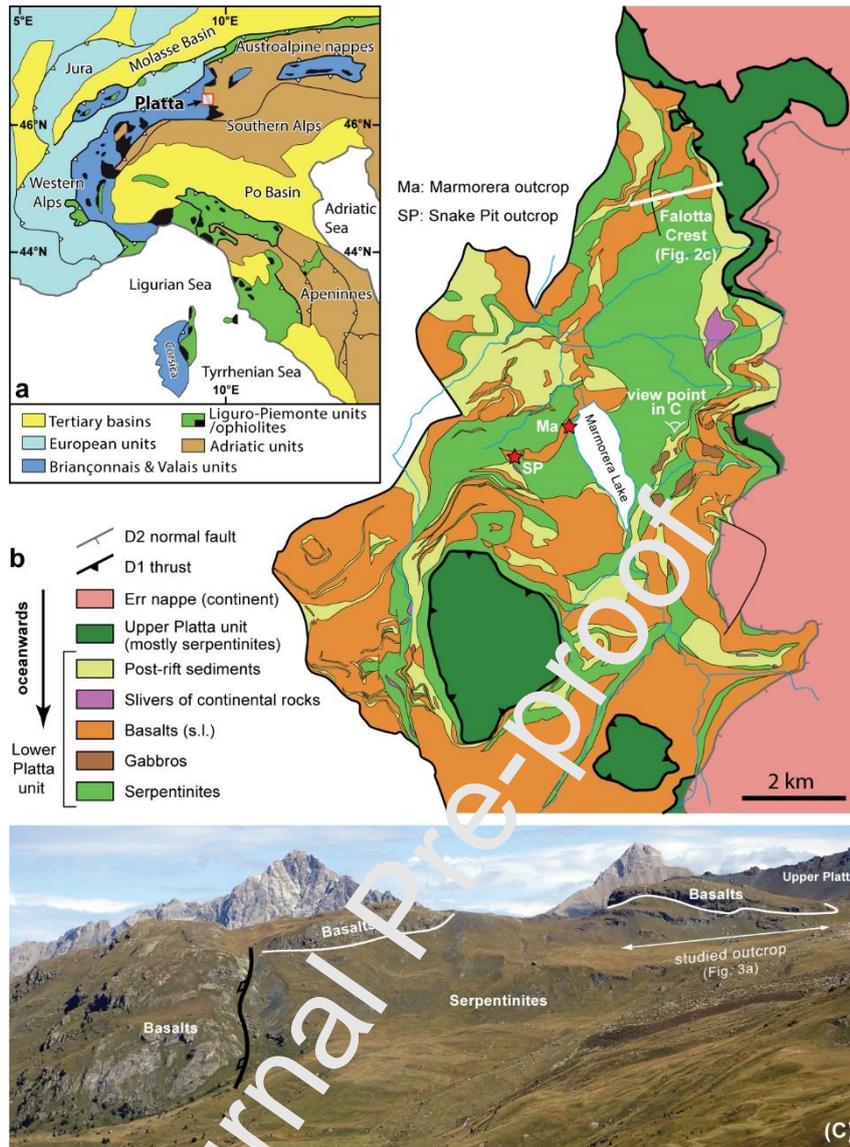
Figure 2. (a) Simplified map of the major paleogeographic units of the Western and Central Alps and, the Apennines. (b) Geological map of the Platta nappe (modified after Schaltegger et al., 2002). Location of the Falotta outcrop (figure 2c) on the northern side of the nappe. Red stars point out the location of established Jurassic detachment plane juxtaposing basalts onto serpentinite where carbonation has been observed (Epin et al., 2019, Coltat et al., 2019b). (c) Roughly E-W oriented section of the Falotta area corresponding to a ~1500m in length of almost continuous crest. On the most eastern part of the landscape, the Upper Platta unit is visible. The studied area corresponds to the eastern part of the crest and is exposed on ~400m long continuous section along which basalts lie on the serpentinized mantle rocks (thin white lines). On the western part of the section, a high-angle normal fault, likely active during Jurassic stretching (thick black line), suggests that the Falotta outcrop corresponds to a horst.

2.2. The Falotta outcrop, previous data

The Falotta outcrop (fig. 3a) is a continue section along the Falotta crest (figs. 2b, c) preserving a basalt-serpentinite interface. It is roughly E-W oriented, over 400 meters laterally and over 100 meters high (fig. 3a). Two sliding blocks (blocks which have slipped from the main cliff) are present in the western part of the section (fig. 3a). Three distinct lithologies can be distinguished that are from bottom to top: serpentinites showing a progressive enrichment in carbonates; forming the so-called ophicalcites and then basalts immediately above (fig. 3a).

The outcrop represents a key section described in several previous studies and the target of classical excursions to visit the Ocean-Continent Transition in the Alps. Indeed, the top of the serpentinized mantle rocks (excluding some patches of sedimentary breccias) is currently interpreted to be a remnant of a regional-scale exhumed and then reworked detachment surface inherited from Jurassic extension (Epin et al., 2017, 2019, Coltat et al., 2019a; Ribes et al., 2019). This statement is based on the sequence of deformation in the serpentinites of Falotta, which resembles the one observed in Tasna (Manatschal et al., 2006). This includes serpentinite cataclasites at the base with a system of anastomosing shear planes, which evolves towards serpentinite gouges embedding rounded serpentine clasts at the top. The top of the sequence is made of tectono-sedimentary breccias (Desmurs et al., 2001) inferred to be the result of the reworking of serpentinized-derived material at the seafloor. Basalts spread onto this level of tectono-sedimentary breccias (i.e. the top of the exhumed detachment surface) and therefore post-date the main phase of detachment-assisted mantle exhumation and its subsequent reworking at the seafloor.

Previous studies have investigated the nature of the interface between the basalts and the serpentinites and proposed that at Falotta, this surface was reactivated by a flat Alpine thrust (Desmurs et al., 2001; Epin et al., 2017, 2019). This interpretation was based on the foliated nature of the rocks along the interface. However, Coltat et al. (2019a), based on petro-geochemical and structural data, recently reinterpreted this interface as inherited from Jurassic extensional tectonics without evidence for a significant Alpine overprint. The present study provides new data supporting this reinterpretation. The whole set of arguments will be presented and discussed below.
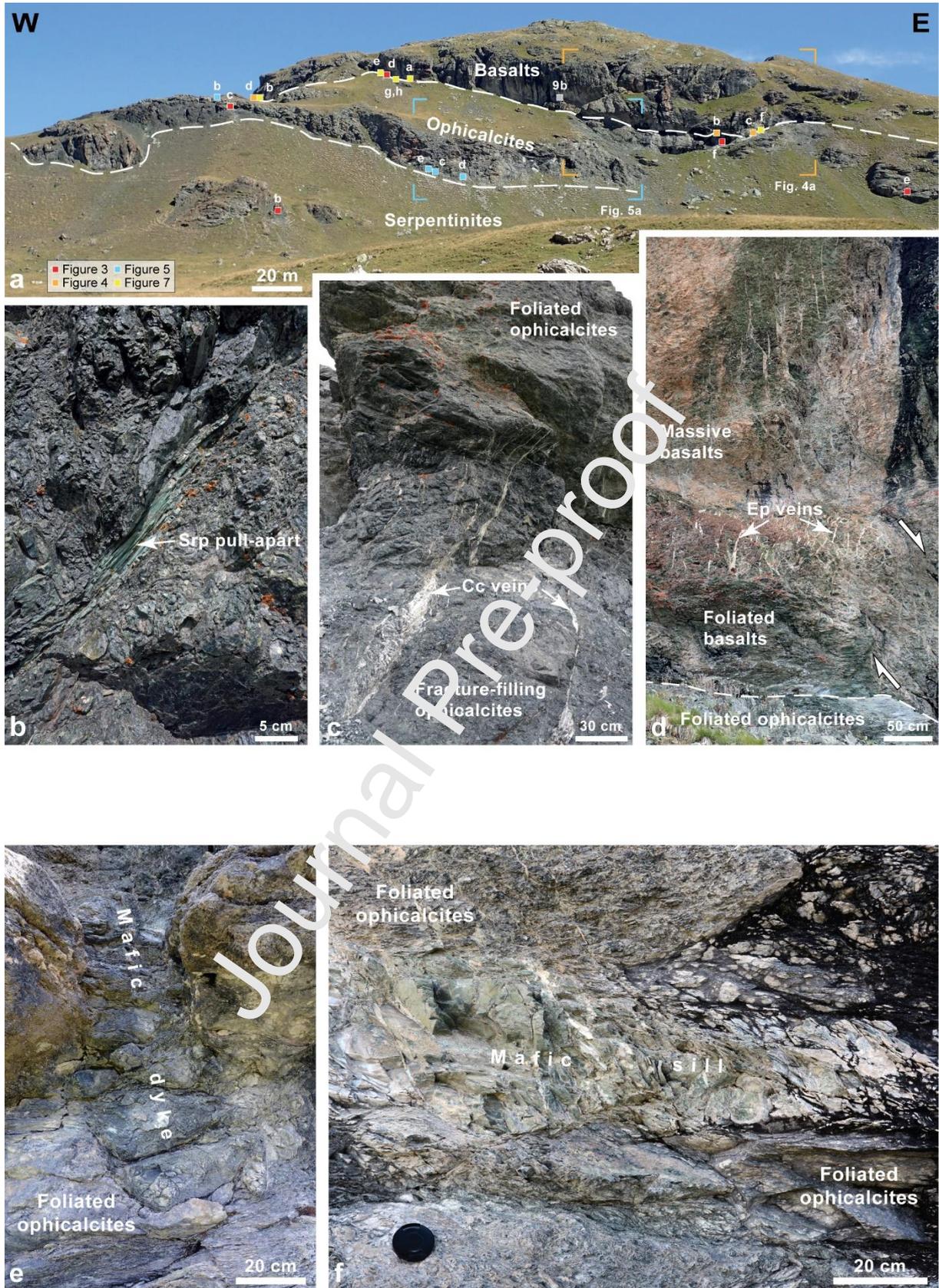
Figure 3. All field pictures displayed are E-W oriented when unspecified. (a) Panorama of the the Falotta outcrop, the dashed white lines define the upper and lower limits of the

ophicalcites. (b) At the base of the section, dark serpentinite cataclasites showing a network of anastomosing shear planes, which encloses undeformed serpentinite lenses. Dark serpentinites are crosscut by shear planes and veins filled with late green fibrous serpentine (Srp) locally forming pull-apart structures. (c) Upwards, calcite veins (Cc veins) cut through serpentinites forming fracture-filling ophicalcites below the sharp contact with the overlying foliated ophicalcites. This contact becomes more gradual towards the east. (d) Foliated basalts and then massive basalts crosscut by greenschist type assemblage veins (Ep veins) lying onto the foliated ophicalcites corresponding to the typical contact between mafic and ultramafic rocks along the section (upper white dashed line on fig. 3a). Note that, as a consequence of alteration, basalts display a light to dark greenish or orangish color. (e) Dismembered mafic dyke in the foliated ophicalcites. (f) Dismembered mafic sill in the foliated ophicalcites. The mafic intrusion is crosscut by calcite veins that propagate into the foliated ophicalcites.

3. LITHOLOGIES OF THE FALOTTA OUTCROP

At the base, the section is made of dark serpentinized peridotites showing advanced serpentinization (figs. 3a, b). The main serpentine species is lizardite, which is locally crosscut by green fibrous serpentine veins (fig. 3b). Locally, mafic intrusions crosscut the serpentinized mantle rocks. Prior to carbonation, during late stages of serpentinization, a deformation gradient is observed in the serpentinite unit. Those structures and textures (e.g. cataclastic shear bands, pull-apart veins filled with green serpentine, gouges) are inherited from a former Jurassic pre-carbonation exhumation related to the activity of detachment systems (see above). This early stage has been described in Epin et al. (2017) and Coltat et al. (2019a) and is not the focus of this study. Mineralogical and structural details about those former stages of extensional tectonics are given in appendix 1.

At the top of the serpentinite unit, calcite veins crosscut the serpentinite gouges and the different serpentine species (fig. 3c). The veins are cm-thick and mostly filled either with rhombohedral or elongated calcite grains. The internal textures of theses veins show no medium zones, frequent slices of wall rocks, inclusion fluid bands and sawtooth-shaped contours of elongated grains. According to Bons et al. (2012), most of these veins are stretching veins with stretched calcite crystals formed during a crack and seal mechanism. Then, in the following sections, we use the term stretched crystal rather than fiber to qualify those elongated calcite grains. Sparsely, blocky and elongate blocky textures are sometimes

encountered also suggesting syntaxial veins at some place. This vein network affects the basal part of the ophicalcite unit and refers to as fracture-filling ophicalcites (Weissert and Bernoulli, 1984). Within the fracture-filling ophicalcites, apart from veins, thin shear bands and thicker fault zones are also carbonated. The amount of calcite veins increases towards the east of the outcrop. There, the matrix becomes pervasively carbonated. Above the fracture-filling ophicalcites, the foliated ophicalcite displays higher carbonate contents (fig. 3c). This contact is sharp in the western part of the outcrop (fig. 3c) and is more transitional towards the east. The foliated ophicalcites are made of serpentinite lenses of various sizes (centimeters up to several meters) wrapped in a foliated calcitic matrix, with late calcite veins (fig. 3f). Dismembered mafic dykes and sills are locally preserved in the foliated ophicalcites (fig. 3e, f). This foliated ophicalcite unit corresponds to "the tectono-sedimentary breccia" unit of Desmurs et al. (2001). Noteworthy, at Falotta, sedimentary breccias and debris flows reworking serpentinite and ophicalcite clasts being embedded within a serpentinite sandy matrix have been identified (Epin et al., 2017; Ribes et al., 2019). Those sedimentary breccias are also affected by pervasive carbonation and form meter-sized lenses embedded within foliated ophicalcites.

The ophicalcite unit is overlain by a mafic extrusive unit composed, from its base to its top, of foliated hyaloclastites, a foliated sole and then massive basalts with some epidote+chlorite+albite+quartz grains associated with late calcite veins (fig. 3d, app. 1g). Hyaloclastites are foliated and display a reddish to greenish color. They occur sporadically at the western and eastern part of the outcrop, with a maximal thickness of 10 meters. Mineralogically, they contain a fine-grained matrix of chlorite and Fe-hydroxides (app. 1e). Locally, ghosts of pyroxene phenocrysts and vesicles are filled with chlorite or an assemblage of chlorite and calcite, respectively (app. 1e). The foliated basaltic sole is 50 cm to 1 m-thick (figs. 3d, 4a, b) and displays a sharp contact with the massive basalts (figs. 3d, 4b). Both hyaloclastites and the foliated sole contain discrete veins made of calcite and chlorite (app. 1e), the latter generally present at the rims of the veins. Massive basalts are made of epidote, chlorite, albite and minor quartz, actinolite, titanite and preserved plagioclase (app. 1g, h). This assemblage points to a high-temperature hydrothermal alteration event (>250°C) likely during the basalt emplacement and was followed by a late carbonation event of about 100°C (Coltat et al., 2019a).

4. STRUCTURES AND FAULT ROCKS

The structures, fault rocks, kinematics and micro-structural features of the Falotta outcrop are shown in figures 4, 5 and 7. The orientation of the structures, their dips and the associated lineations are shown in figure 6.

4.1. The basalt-ophicalcite contact

The nature of the basalt-ophicalcite contact can be better assessed from the eastern part of the Falotta outcrop (fig. 4a). The contact is sharp and is strongly tectonized (figs. 4b, c). As such, this contact constitutes a sub-horizontal decoupling level between basalts and serpentinized mantle rocks. No evidence of ductile strain (e.g. dynamic recrystallization, pressure solution creep, crystal plasticity) has been documented along the contact. Rather, cataclastic flow is the dominant mechanism. Therefore, we consider the structures occurring at the decoupling level as low-angle faults rather than shear zones. These low-angle faults show a normal sense of shear with locally opposite kinematics (fig. 4a). These structures are associated with an intense fluid circulation (e.g. numerous veins, figs. 4b, c).

4.2. Structures in the basalts

Within the foliated basalt sole, the foliation is marked by a pervasive assemblage of chlorite and actinolite defining a planar fabric. This flat foliation is not homogeneously distributed laterally as some areas represent massive basalts (fig. 4c), which preserved typical volcanic textures such as spherulites (app. 1f). The discrete calcite+chlorite veins are folded with axial fold planes parallel to the bulk foliation in the basalts. Locally, axial planes are underlined by a chlorite rich axial foliation with elongated chlorite grains crossing the vein (fig. 7d). Elongated chlorite and calcite grains do not present internal strain (fig. 7d).

The whole basalt unit is affected by high-angle faults in apparent conjugate systems (figs. 4b-d). They locally present several orientations of slickensides (fig. 4c). Where present, slickenlines have high pitch values, indicating a small amount of oblique slip (fig. 4c). Dip values of fault planes, slickensides kinematic criteria and offsets indicate normal faulting unequivocally. Downwards, these normal faults branch into the low-angle normal fault zones, rooting within the foliated ophicalcites and then crossing and offsetting (with a normal sense-of-shear) the foliated basaltic sole (figs. 4b, c).

In massive basalts, veins are steeply-dipping and locally branch on the high-angle normal faults (fig. 4b). Locally, veins form either oriented stockworks (fig. 3d) or a "mosaic"

hydrothermal cataclasite, where the vein frequency is higher. Some core zones of high-angle normal faults are made of hydrothermal gouges (fig. 4d), whereas the damage zone corresponds to a mosaic hydrothermal cataclasite. The gouge, made of crushed basaltic materials, is intensively replaced and cemented by an assemblage of tiny grains (~ 50-300 µm) of calcite, hydroandradite, actinolite and talc. An internal foliation oblique to the wall rock is defined by the phyllosilicates and indicates a normal sense-of-shear (fig. 4d).
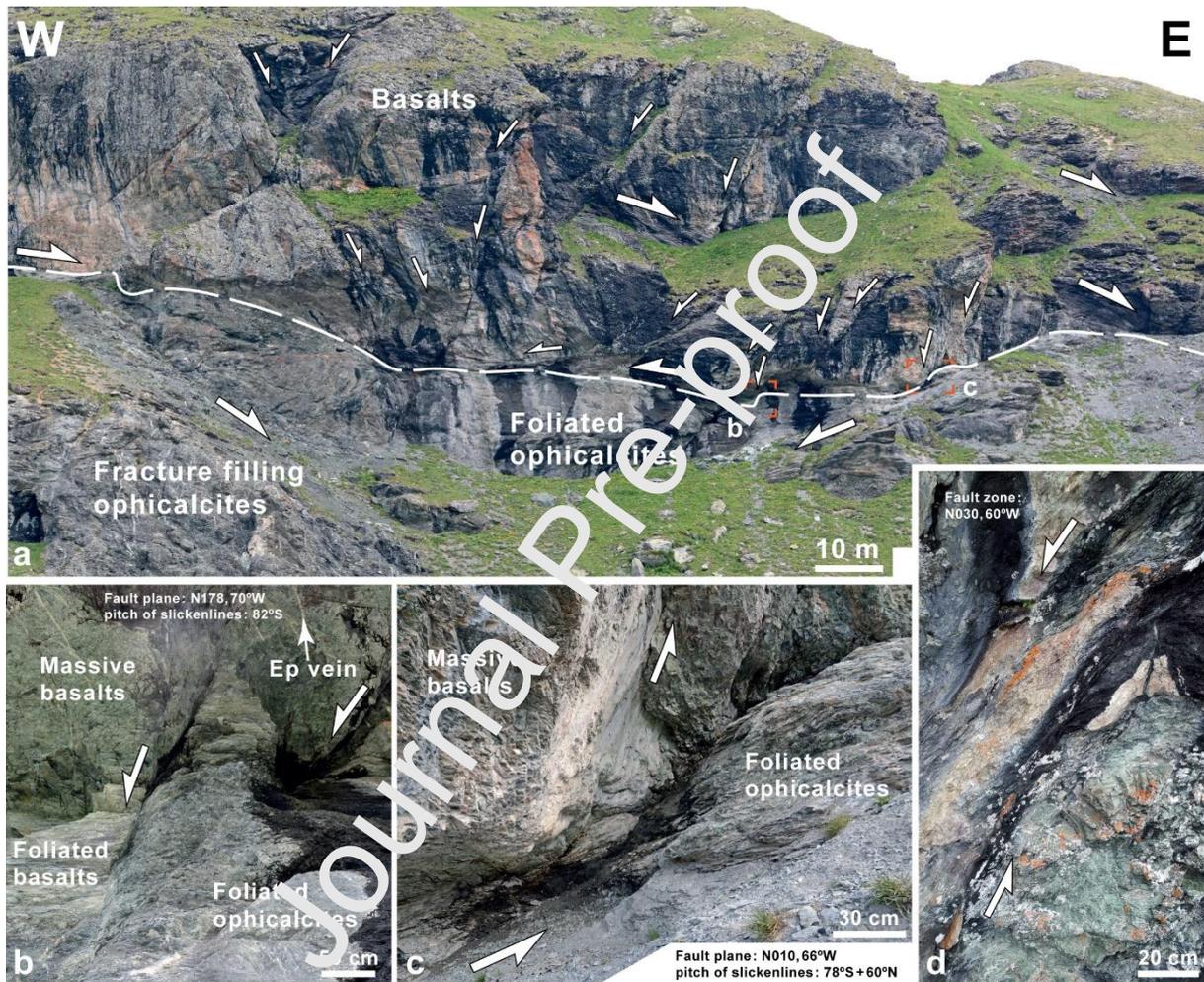

Figure 4. (a) General view of the eastern part of the Falotta section. The contact between foliated ophicalcites and basalts is underlined by the dashed white line. Most of the high-angle normal faults are synthetic with respect to the underlying low-angle normal fault. (b) N-S oriented top-to-the-west high-angle normal faults cutting through massive and foliated basalts and rooting into the foliated ophicalcites. Greenschist type assemblage veins (Ep veins) are connected to fault planes and their dip and orientation are compatible with fault kinematics. (c) N-S oriented, top-to-the-west high-angle normal fault cutting through massive basalts and rooting in a top-to-the-west low-angle normal fault within the foliated ophicalcites. Two generations of slickenlines are observed. (d) Hydrothermal gouge

developed in the core of a roughly NNE-SSW oriented, top-to-the-west to northwest high-angle normal fault affecting the chloritized basalts (location fig. 4a). Structural data are written using the strike and dip representation.

4.3. Syn-carbonation structures and fault rocks within ophicalcites

In the ophicalcite unit (fig. 5), three main structures are observed: i) the foliated bands (figs. 3c, 4b, 5b) which are dominant structures in the upper part of the unit. In contact with the overlying basalts, they define anastomosed and foliated thick calcite-rich (up to 70 % vol.) zones embedding millimeter- to tens of centimeter-long preserved clasts of serpentinite; and ii) calcitic shear bands corresponding to thin bands of carbonated fault rocks, locally associated with veins and frequently distributed in conjugate systems (figs. 5a, b, e, f); the shear bands confer the anastomosed pattern of the thicker foliated bands; and iii) fault zones which are thick zones of carbonated fault rocks between two wall rocks (figs. 5a, c). In the ophicalcites, the density, the thickness and the carbonate content of these three structures increase upwards from the basal carbonation front (fig. 3a). The fault rock material is made of a foliated matrix containing tiny grains of calcite (~10-50µm) and minor hydroandradite, talc, actinolite and preserved clasts of crushed serpentinite or isolated rhombohedral calcite (app. 1d). The serpentinite clasts are then surrounded by a calcitic cement and are locally crosscut by calcite veins. Commonly, remnants of serpentine partially chloritized and primary peridotite-derived mineral phases are also present in the matrix.

Downwards, in the fracture-filling ophicalcites, calcite veins either root into or are crosscut by calcitic shear bands (figs. 5e, f). Calcite grains present in the veins are either blocky (coarse grains up to several centimeters in size) or stretched crystals. Offsets and geometry relationships between calcite stretched crystals and vein wall-rock allow to define two types of veins: i) extensional veins (fig. 5e, mode I) and ii) hybrid shear extensional veins (figs. 5d-f, mode II). There is no relationship between a particular habit and a type of vein. Veins also contain minor chlorite, which is present at the rims replacing serpentine (fig. 5g). In the eastern part of the outcrop, the conjugate calcite vein pattern associated with conjugate shear bands results in individualization of rounded serpentinite clasts surrounded by calcite veins, thus defining "cockades" (e.g. Berger and Herwegh, 2019). This pattern represents a crack and shear cockade breccia texture (fig. 5f). Calcite shear veins are thin both above and below the clast and thicker laterally where vein segments correspond to pure extensional veins (i.e. calcite stretched crystals are sub-perpendicular to wall rocks). This crack and shear cockade breccia pattern is also expressed at a microscopic scale in fracture-filling

ophicalcites, where discrete calcite veins with stretched crystals surround serpentinite clasts (fig. 5g).
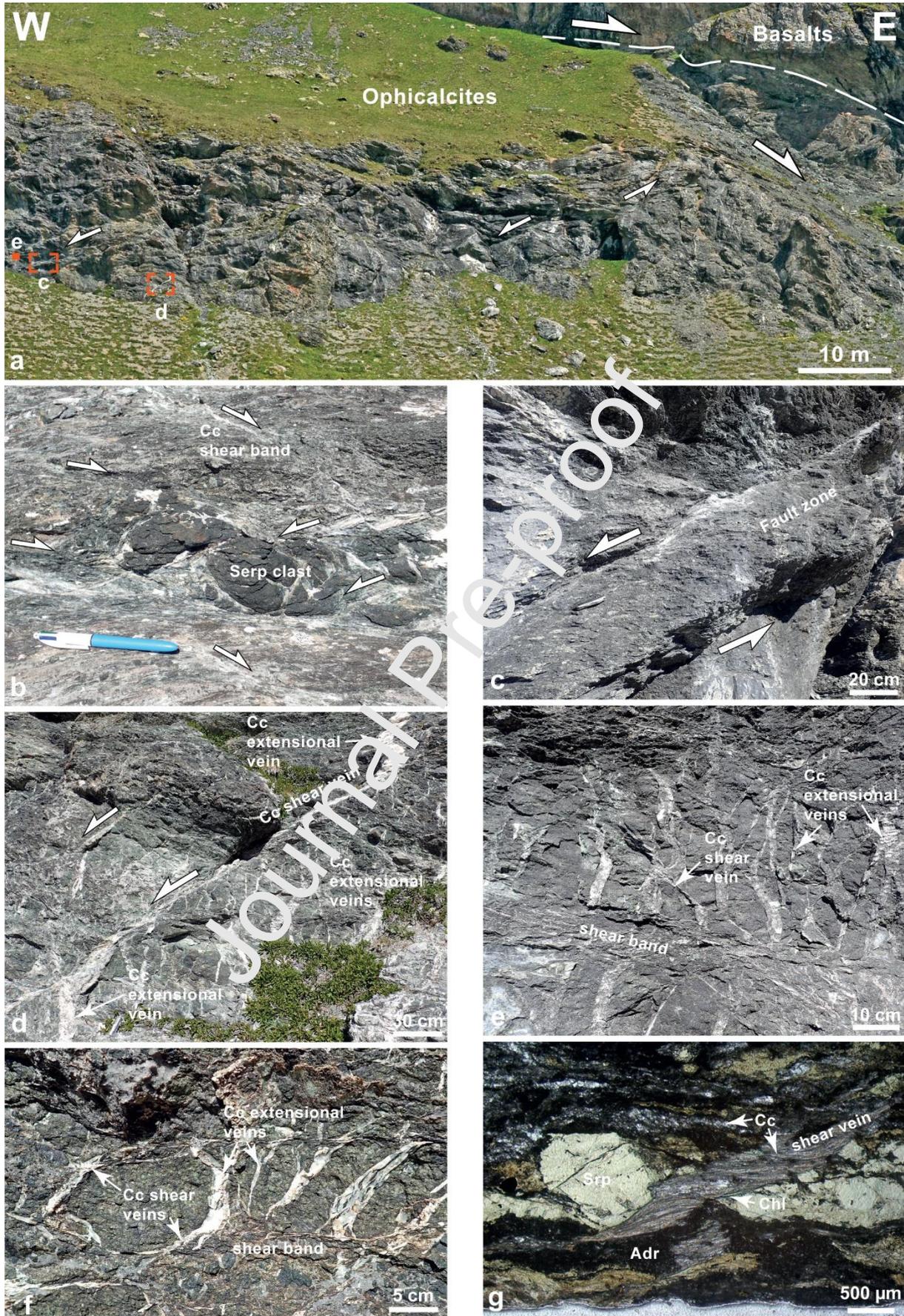
Figure 5. Main structures observed into the ophicalcites, all photographs are W-E oriented and sub-vertical, see location on fig. 3a. (a) Enlargement on the middle part of the Falotta outcrop where ophicalcites are overlain by basalts. (b) Horizontal thick foliated bands affected by conjugate calcitic shear bands surrounding a serpentinite clast in the foliated ophicalcites. Calcite veins develop parallel to shear bands and also crosscut the serpentinite clast. (c) Meter-thick carbonated fault zone at the transition between the foliated ophicalcites and the underlying fracture-filling ophicalcites; (d) Top-to-the-west calcite shear vein in the fracture-filling ophicalcites, which appears to be a relay zone between two slightly folded extensional veins; (e) Network of calcite extensional veins and calcite shear veins truncated by sub-horizontal calcitic shear bands into the fracture-filling ophicalcite sub-unit. (f) Typical cockade pattern. Veins root inside a sub-horizontal calcitic shear band. (g) Microscopic views of the fracture-filling ophicalcites presenting the cockade pattern observed at a larger scale in (f). Calcite (Cc) veins with minor chlorite (Chl) wrap around serpentinite clasts. Hydro-andradite (Adr) accompanies carbonation of the serpentinites. Cc=calcite, Srp=serpentine.

5. DEFORMATION ANALYSIS

5.1. Structure strikes and dips

In the ophicalcites (fig. 6), extensional veins (EV) and hybrid shear extensional veins (SV) are roughly N-S oriented ($\pm40°$ of dispersion around this value). Generally, EV are steeply-dipping ranging from 60° to 90° with an average around 80° whereas SV are more gently-dipping. In the fracture-filling ophicalcites, veins either dip towards the east or the west. Calcite stretched crystals in these veins display ENE-WSW orientations and are almost horizontal to gently-dipping (average around 20° with a full range from 0° to 60°). In the foliated ophicalcites, the veins are generally more gently-dipping. The flattening of the calcite veins towards the basalt unit is consistent with a strain localization along low-angle faults. In the eastern part of the section, the veins do not show any preferential dip direction while they preferentially dip towards the west or the east in the western and central part of the section, respectively. The changes of preferential dip directions of veins in the foliated ophicalcites is also indicative and coherent with opposite kinematics along low-angle faults at the basalt-ophicalcite interface. Calcitic shear bands (SB) are roughly N-S oriented ($\pm40°$ of dispersion around this value) and are sub-horizontal to gently-dipping (up to 50°). In the fracture-filling ophicalcites, most of the SB are sub-horizontal, making it difficult to determine a preferential

dip direction. In the foliated ophicalcites from the western and eastern parts of the outcrop, the SB roughly dip towards the east, whereas they dip towards the west in its central part. Those changes of preferential dip directions of SB are coherent with the changes of kinematics along the low-angle faults at the basalt-ophicalcite interface.

In the basalts, EV display NNE-SSW orientations and are steeply-dipping (average around 80°). SV from the western part of the section are roughly NNE-SSW oriented. Two populations can be distinguished dipping either towards the northwest or the southeast. SV from the central part of the section dip unequivocally towards the east-southeast. These dip directions are consistent with those reported for the veins in the underlying foliated ophicalcites. SV have not been reported in the eastern part of the outcrop. Foliation planes (FP) measured in the foliated basaltic sole are sub-horizontal to low-dipping along the outcrop. Stretching lineations measured on FP display E-W orientations in the western part of the outcrop and are more dispersed eastwards. Finally, fault planes measured in the eastern part of the outcrop show NNW-SSE to NNE-SSW orientations and are steeply-dipping towards the west. Striations measured on these planes are roughly along dip direction.

We collected structural data along a cross section through the northern face of the Falotta outcrop (i.e. behind the southern face presented in this paper, fig. 6). Along the cross section, most of the outcrops are composed of basalts with basal reddish foliated hyaloclastites. EV and SV are roughly N-S oriented and are steeply-dipping or more gently-dipping towards the east, respectively. FP are low-dipping towards the north. These orientations measured along the cross section are coherent with those reported along the Falotta southern face.
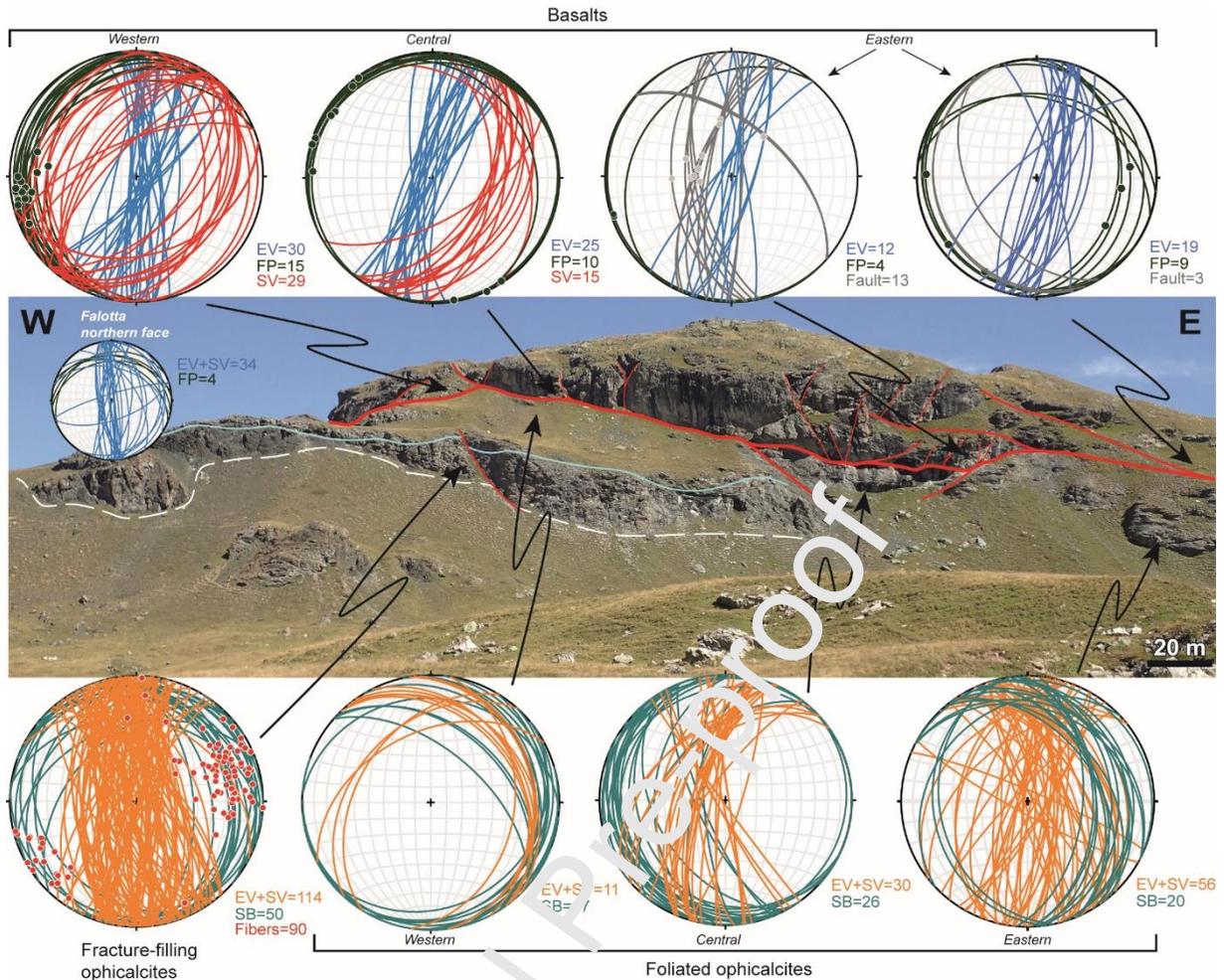
Figure 6. Falotta outcrop line-drawing with structural analysis plotted in stereograms (equal area, lower hemisphere, number of measurements indicated for each structures). Stereograms at the top in the basalts: extensional vein planes (EV, blue curves), shear vein planes (SV, red curves), fault planes and striations (grey curves with grey dot), foliation planes and lineation (FP, dark green curves and dots). Stereograms at the bottom in the ophicalcites: extensional and hybrid shear-extensional vein planes (EV+SV, orange curves), calcite stretched crystals in EV+SV ("fibers", red dots), shear bands and lineations (SB, green curves and dots). The stereogram on the line drawing corresponds to data (foliation planes and EV+SV) collected in the basalts along the northern face of the Falotta crest including the western and eastern edges of the cliff.

5.2. Kinematics and micro-structural data along the basalt-serpentinite interface

In the basalts, from the western part of the outcrop, en-echelon arrays of extensional veins rooting in the foliated basaltic sole display a top-to-the-west sense of shear (fig. 7b). Similar kinematics have been deduced from the internal oblique foliation of the hydrothermal

gouge in high-angle normal fault cutting through massive basalts (fig. 4d). The same kinematics can be deduced at the microscale from sigma clasts in the hyaloclastites (fig. 7c). Conversely, in the central part of the outcrop, all structures present a top-to-the-east sense of shear. Typical en-echelon vein arrays show distinct top-to-the-east sense of shear in the massive basalts (fig. 7a). Similar kinematics are deduced from the shear bands in the foliated basalts (fig. 7e). Also, discrete hybrid shear-extensional veins encountered in this zone show a top-to-the-east sense of shear (fig. 7d). In the eastern part of the outcrop, relationships between high-angle and low-angle normal faults indicate a top-to-the-west sense of shear (figs. 4b, c).

In the ophicalcite unit, kinematics can be deduced from calcitic shear bands (figs. 5b, 7f, h), fault zones (fig. 5c), calcite pull-apart (fig. 7g) or calcite shear veins (figs. 5d, g). Along the low-angle fault zones, the foliated ophicalcites show coherent kinematics with those observed in the overlying basalts: i) in the central part of the outcrop, at the interface with the basalts, both pull-apart structures (fig. 7g) and calcitic shear bands (fig. 7h) show a top-to-the-east sense of shear; and (ii) from the eastern part of the outcrop, a change in sense of shear is visible passing to top-to-the-west kinematics deduced from the shear bands (fig. 7f). Downwards in the low-angle normal faults, the sense of shear criteria is rather diagnostic of co-axial strain: i) the foliated ophicalcites present conjugate normal shear bands (fig. 5b); and ii) below in the fracture-filling ophicalcites, a dominant kinematic is difficult to establish. For instance, most of sense of shear criteria indicate top-to-the-west kinematics (figs. 5c, d, g) while top-to-the-east kinematics are equally expressed (i.e. from SB displayed in fig. 6).

At the scale of the outcrop, the changes of the sense of shear define a conjugate system with major structures (i.e. low-angle normal faults at the basalt-serpentinite interface) dipping either towards the east or the west. Four main segments of low-angle normal faults have been recognized; two dipping towards the east and two others dipping towards the west. Nevertheless, it is difficult to assess the inversion point of sense of shear along this low-angle fault system and hence the crosscutting relationships between top-to-the-east and top-to-the-west structures since they are rare. However, from the main structures, it appears that top-to-the-west structures are crosscut by top-to-the-east structures. This is inferred by the fact that at a large scale, the main top-to-the-west structures do not continue laterally, whereas the top-to-the-east structures are visible and propagate into the basalts (figs. 6 and 8).

Figure 7. Kinematics at the basalts-serpentinite interface along conjugate systems of low-angle normal faults at Falotta; all photographs are vertical and W-E oriented, location on fig. 3a. (a) Typical en-echelon array of extensional veins filled with epidote and late calcite affecting epidotized and chloritized massive basalts, top-to-the-east sense of shear. (b) Similar en-echelon vein array rooting into the chloritized foliated basaltic sole with a top-to-the-west sense of shear. (c) Porphyroclast replaced by chlorite with a top-to-the-west sense of shear in the hyaloclastites at the base of the basaltic unit. (d) Discrete calcite (Cc)+chlorite (Chl) vein from the foliated hyaloclastites with a well-developed chlorite-rich schistosity

passing through the vein in which elongated chlorite grains crystallized. Drusy calcite does not present textural evidence of dynamic recrystallization. (e) Top-to-the-east sense of shear deduced from relationships between gently-dipping shear bands and foliation at the basaltic sole. The transition with overlying massive basalts is sharp. Greenschist type extensional veins with late calcite in the massive basalts root into the foliated sole. (f) Shear bands-foliation relationship in the foliated ophicalcites and geometrical relations with the overlying basalts. Top-to-the-west sense of shear. (g) Top-to-the-east sense of shear deduced from a calcite pull-apart relaying calcitic shear bands in foliated ophicalcites at about 30 cm beneath the contact with the basalts. (h) Calcitic shear band-foliation relationships showing a top-to-the-east sense of shear in the foliated ophicalcites.

6. INTERPRETATION: A CO-AXIAL DECOUPLING LEVEL BETWEEN BASALTS AND SERPENTINITES

Based on those petrological and structural geological data we present in figure 8 an interpreted cross-section of the Falotta outcrop.

The first result is that all the structures of the basalt-serpentinite interface at Falotta are subtractive and therefore characterize a horizontal stretching. In the basalt unit, both top-to-the-west and top-to-the-east low-angle normal faults zones are associated to steeply-dipping normal faults, forming a conjugate system at some places (figs. 4c, 7c, 8). Those high-angle normal faults branch into the low-angle normal faults at the basalt-serpentinite interface either with a listric curve without offset of the foliated basaltic sole (fig. 4c), or crosscutting the foliated basaltic sole inducing a small offset (fig. 4b). In both cases, these high-angle normal faults are mostly synthetic to the underlying low-angle normal faults even though locally, antithetic faults may be observed. Downwards, the ophicalcites present: (i) similar subtractive structures with a normal sense-of-shear as shear veins, shear bands, fault zones, and (ii) extensional veins, all diagnostic of horizontal stretching (fig. 5).

The second result is that this horizontal stretching is usually W-E oriented. Also, the important overlap between the orientation of the structures in the ophicalcites and in the basalts (fig. 6) supports that both units underwent the same W-E horizontal stretching. Driving forces of this deformation (e.g. crustal extension vs. gravity-driven processes) are discussed below.

A third result is that W-E horizontal stretching is achieved though bulk co-axial deformation. Indeed, along the basalt-serpentinite interface at least four segments of low-angle normal faults with alternating sense of shear have been identified (fig. 8). The corresponding changes of sense of shear of high-angle normal faults branching into these low-angle fault segments have also been established, resulting in a conjugate system of normal faults with grabens and horsts. Those low-angle normal faults represent zones where maxima of non-co-axial strain is localized. In the ophicalcites, the strain is more distributed and corresponds to conjugate top-to-the-west and top-to-the-east shear bands and shear veins associated with and relaying sub-vertical extensional veins (figs. 5, 6). Therefore, with exception of the uppermost part, the ophicalcites record a co-axial W-E horizontal stretching. Below the intersection of low-angle normal faults, the foliated ophicalcite footwall forms dome-like "roll-under" structures (fig. 8b) with an internal pattern of conjugate anastomosing shear bands. It appears that top-to-the-east low-angle normal faults crosscut top-to-the-west ones (fig. 8). However, we do not interpret those relationships in terms of polyphase tectonic deformation and propose that they rather form a conjugate system (i.e. quasi synchronous). Downward within serpentinites, the rooting of these low-angle normal fault zones is not directly observable; a point discussed below.

Consequently, the roughly flat interface between basalts and serpentinites of the Falotta outcrop corresponds to a co-axial decoupling level during an E-W horizontal stretching. This deformation was assisted by important fluid flow responsible for greenschist facies-type hydrothermal alteration and subsequent carbonation. As represented in the figure 8, this decoupling level can be viewed as the core of a deformed zone composed of foliated ophicalcites and foliated basalts (including foliated hyaloclastites) separating an upper damage zone (veined and massive basalts) from a lower damage zone (fracture-filling ophicalcites).

Finally, since high-angle normal faults and low-angle faults develop at and truncate the basalt-serpentinite interface, this system postdates mantle exhumation at the seafloor. Also, it has to be syn- to post-spreading of mafic extrusives onto the Jurassic seafloor. Therefore, as the top of serpentinized mantle rocks at Falotta is currently interpreted to be a remnant of a regional-scale exhumed detachment surface inherited from Jurassic extension (Epin et al., 2017, 2019), from our data we infer that during magmatism, this Jurassic detachment surface has been reactivated as a decoupling level assisted by important fluid flow responsible for hydrothermal alteration of serpentinized mantle rocks and basalts.
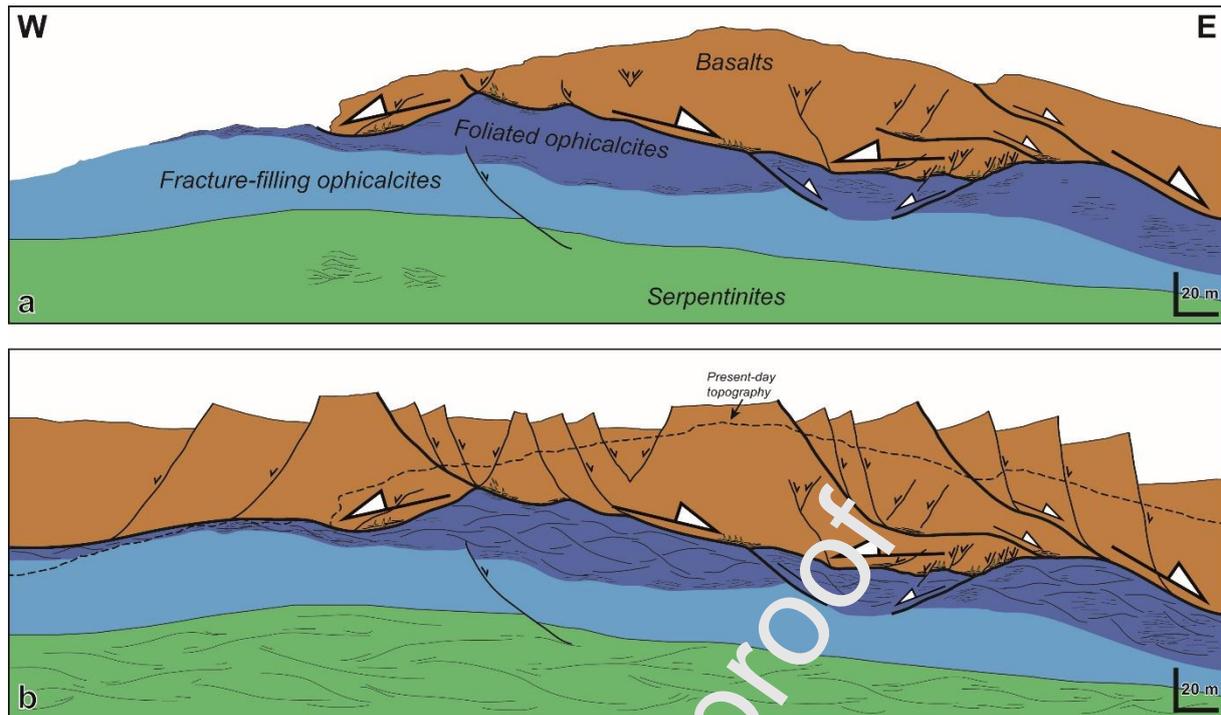
Figure 8. Raw (a) and interpreted (b) cross-sections of the Falotta outcrop. The system is roughly symmetric and shows co-axial deformation marked by the development of opposite vergent low-and high-angle normal fault zones. The roughly flat interface between basalts and mantle rocks (foliated basaltic sole and ophicalcites) acts as a co-axial decoupling level during W-E oriented horizontal stretching. Note that in (b) the top of the basalts represents the seafloor even though the maximum basalt pile thickness remains unconstrained.

7. DISCUSSION

7.1. Preservation of the Jurassic oceanic system in an Alpine ophiolite

The following points allow to constrain the tectonic setting responsible for the deformation structures observed at Falotta: (1) all structures (extensional veins, shear veins, foliated bands, high- and low-angle normal faults) point to a horizontal stretching coeval with fluid circulation along the basalt-serpentinite interface (fig. 6); (2) some of the high-angle normal faults crosscutting the basalts root into the zone of flat-lying foliations, with similar kinematics (i.e. the low-angle normal faults, fig. 4c); (3) other high-angle normal faults crosscut and sometimes deflect (drag folding) the zone of flat-lying foliations (fig. 4b), which confirms that this foliation was not formed during a later tectonic event; (4) no additive structures (i.e. thrusts, reverse shear planes or faults) are observed. Gently-dipping shear veins never present a reverse sense of shear; and (5) the overall conjugate system defined by low-angle normal faults with opposite sense of shear (fig. 8) is indicative of co-axial horizontal

stretching during extensional tectonics rather than thickening controlled by thrusts which mostly generate non-co-axial strain patterns. Altogether, these arguments are diagnostic of extensional tectonics. This precludes the compressional D1 and D3 Alpine phases to be responsible for the observed structures along the basalt-serpentinite interface.

The development of extensional structures may relate to Jurassic rifting or to the D2 Alpine phase, although D2-related structures are known in the Austroalpine units east of the Platta nappe but not in the nappe itself (see geological setting). Petro-geochemical data from the Falotta outcrop, discussed by Coltat et al. (2019a), allow to decide between these two options: (1) isotopic signatures of carbonates forming fracture-filling and foliated ophicalcites and veins in basalts are compatible with typical present-day oceanic ophicalcite signatures. These signatures are very homogenous throughout the basalt-serpentinite interface, which is unlikely in the case of re-equilibrium conditions during a long-lived regional metamorphic event; (2) greenschist type alteration of the deformed basalts (chlorite, epidote and albite) is symptomatic of marine metasomatism under temperatures at about 250-400°C in divergent oceanic contexts; and (3) hydro-andradite associated with calcite either into high-angle normal faults crosscutting the basalts (fig. 4h) or in ophicalcites (fig. 5g, app. 1d) is typical of a low-T hydrothermal circulation during marine metasomatism. These three arguments indicate that fluid-assisted deformation recorded at Falotta are the result of Jurassic extensional tectonics. Also, the W-E horizontal stretching, documented in the Falotta outcrop, is coherent with the Jurassic extension direction reported from the Alpine Tethys rifted margin (Froitzheim and Manatschal, 1996).

The lack of compressional structures may be surprising. The excellent mineralogical and structural preservation of the Falotta outcrop may be due to the moderate burial during the main D1 Alpine phase. This led to a very heterogeneous Alpine overprint, leaving large areas where Alpine tectonics and metamorphism are absent (Epin et al., 2017). In addition, serpentinites of the Upper Platta unit likely acted as a soap layer, which accommodated the main deformation during nappe stacking. This likely prevented the Lower Platta unit to undergo a strong overprint.

7.2. Fluid-rock-deformation interactions

In the basalts, most of the structures record an intense fluid circulation leading to epidotization and chloritization of the rocks (fig. 9a). Noticeably, the foliated sole was altered to chlorite and actinolite whereas the upper part was mostly epidotized (fig. 9b). Based on the

petrographic investigation, the primary feldspars do not indicate any alignment suggesting that this fabric was not inherited and acquired under sub-solidus hot conditions when basalts were emplaced onto the seafloor. Therefore, at the scale of the outcrop, fluid-assisted deformation likely occurred during solid-state conditions when basalts were already spread and cooled onto the seafloor. During this greenschist facies type metasomatism, the upper part of the basalts was more competent than the base and broke in response to horizontal stretching. This rheological limit between the chlorite-rich foliated sole and the overlying epidote-rich damage zone may be very sharp (figs. 7e, 9a) and is probably controlled by complex feedback reactions between deformation- and reaction-induced permeabilities. Such mineralogical zonation has been reported in other magma-rich ophiolites (e.g. Troodos; Richardson et al., 1987).

A late hydrothermal fluid evolution is recorded through the carbonation of the rocks; with a reopening of the former veins (fig. 9b) and the carbonation of the fault rocks and gouges within the fault zones (fig. 4d). The successive paragenesis of those veins (i.e. a primary chlorite+epidote+albite±quartz assemblage followed by a re-opening with late calcite fillings, see Coltat et al., 2019a) indicates that E-W horizontal stretching lasted from conditions of marine greenschist facies metasomatism (~ 250°C) to lower temperatures of carbonation (~ 100°C, see Coltat et al., 2019a). In the veined damage zone, veins define conjugate sets of en-echelon extensional veins in close relation with conjugate shear veins (e.g horse tail termination, fig. 9b), indicating that the bulk brittle deformation within basalts was co-axial, even above a non-coaxial segment of low-angle normal faults (fig. 9a). In the foliated basaltic sole, folded calcite veins with elongated chlorite grains growing parallel to the rock foliation in axial planes attest that fluid circulation was synchronous to extensional deformation. As a consequence, veins formed and folded synchronously with on-going E-W horizontal stretching and associated vertical flattening leading to this noticeable texture (fig. 7d). Such particular features were likely favored by the "softening" of the basaltic sole during intense chloritization and subsequent flattening and foliation development.

Within the foliated ophicalcites, a roughly asymmetrical deformation is visible at the interface with the basaltic unit (fig. 9a). This is visible one to two meters below the contact with the basalts and it is pointed out by both shear band-foliation relationships and pull-apart structures (fig. 7). Downwards, the deformation becomes roughly co-axial (fig. 9a) leading to a symmetrical anastomosed strain pattern. There, the carbonate content of the rocks is high (>70%) and attests that the maximum of fluid flow was channelizing along this level. The

foliated calcitic cement surrounding serpentinite clasts does not show any traces of dynamic recrystallization. Together with multi-scale calcite-filled veining, this argues for a deformation achieved through cataclastic flow. From this mechanical aspect, the foliated ophicalcites correspond to a thick level of carbonated gouges. This is consistent with the fact that these rocks were at shallow depth (several tens to hundreds of meters below the paleo-seafloor) during the deformation event.

The transition with the fracture-filling ophicalcites is marked by carbonated and conjugate normal fault zones (figs. 5c, 9a). Downwards, fracture-filling ophicalcites present a broad regular N-S oriented set of extensional and shear veins (fig. 6). The co-axial strain regime is expressed through conjugate shear veins and shear bands leading to the formation of a particular ophicalcite breccia facies, here named crack and shear cockade breccias (figs. 9b, c).

Crack and shear cockade breccias are informative about fluid pressures, differential stresses and the role of pre-existing anisotropies during the activity of the decoupling level (fig. 9d). Indeed, with respect to horizontal the stretched calcite crystals ("fibers" in fig. 9c) in veins segments surrounding serpentinite clasts (figs. 9c, d) such brecciated patterns indicate W-E horizontal stretching. Vertical and horizontal symmetry of stretching calcite veins surrounding the clasts indicate a conjugate and curved extensional to hybrid shear-extensional vein system. This vein pattern cannot be explained without invoking within the serpentinites the role of inherited anastomosed conjugate shear bands (with non-cohesive gouges) separating elongated lenses of more cohesive serpentinites. In a Mohr circle graphic representation, such crack and shear cockade breccias form both in the tensional field (extensional and shear veins, point 1 and 2, figs. 9d, e) and in the compressional field by reactivation of existing cohesionless shear planes at high-angle with the vertical main principal stress (i.e. $\sigma 1$, point 3 on fig. 9d, e). Therefore, we propose that the inherited pattern of conjugate shear bands containing crushed serpentinite matrix (i.e. non-cohesive gouges) was reactivated during syn-carbonation deformation and led to the crack and shear cockade breccias. Tensile failure is thus possible in cohesive serpentinite lenses between the conjugate set of non-cohesive shear bands. This interpretation implies low differential stresses and fluid pressures overcoming the horizontal main principal stress (i.e. $\sigma_{effective} 3 = \sigma'3 < 0$ and close to the tensile strength of serpentinites, see fig. 9e). In such a shallow crustal context (mafic extrusives overlying exhumed serpentinized mantle rocks below sea level), low differential stresses are expected. Assuming reasonable water depths (>2000 m) above a porous basalt pile (500m-thick at first

approximation) conditions, the resulting fluid pressure at 2500 m (i.e. at the decoupling level depth) is of about 25 MPa and the lithostatic pressure (i.e $\sigma_v = \sigma_1$ obtained by addition of 2000 m water column plus 500 m of hydrated basalts with a density of 3.10^3 kg.m^{-3}) is of about 35 MPa. The effective vertical stress is then of about 10 Mpa (fig. 9e). In these pressure conditions, synchronous modes 1, 2 and 3 cracking are coherent with published failure envelopes for massive serpentinites and cohesionless serpentinite gouges (fig. 9e). Consequently, significant water depth and basalt thickness in an ultra-distal rifted margin yield favorable mechanical and hydraulic conditions for the reactivation of a former mantle gouge overlain by a submarine basaltic pile. Noteworthy, this mechanical solution does not require necessary supra hydro-static fluid pressures.
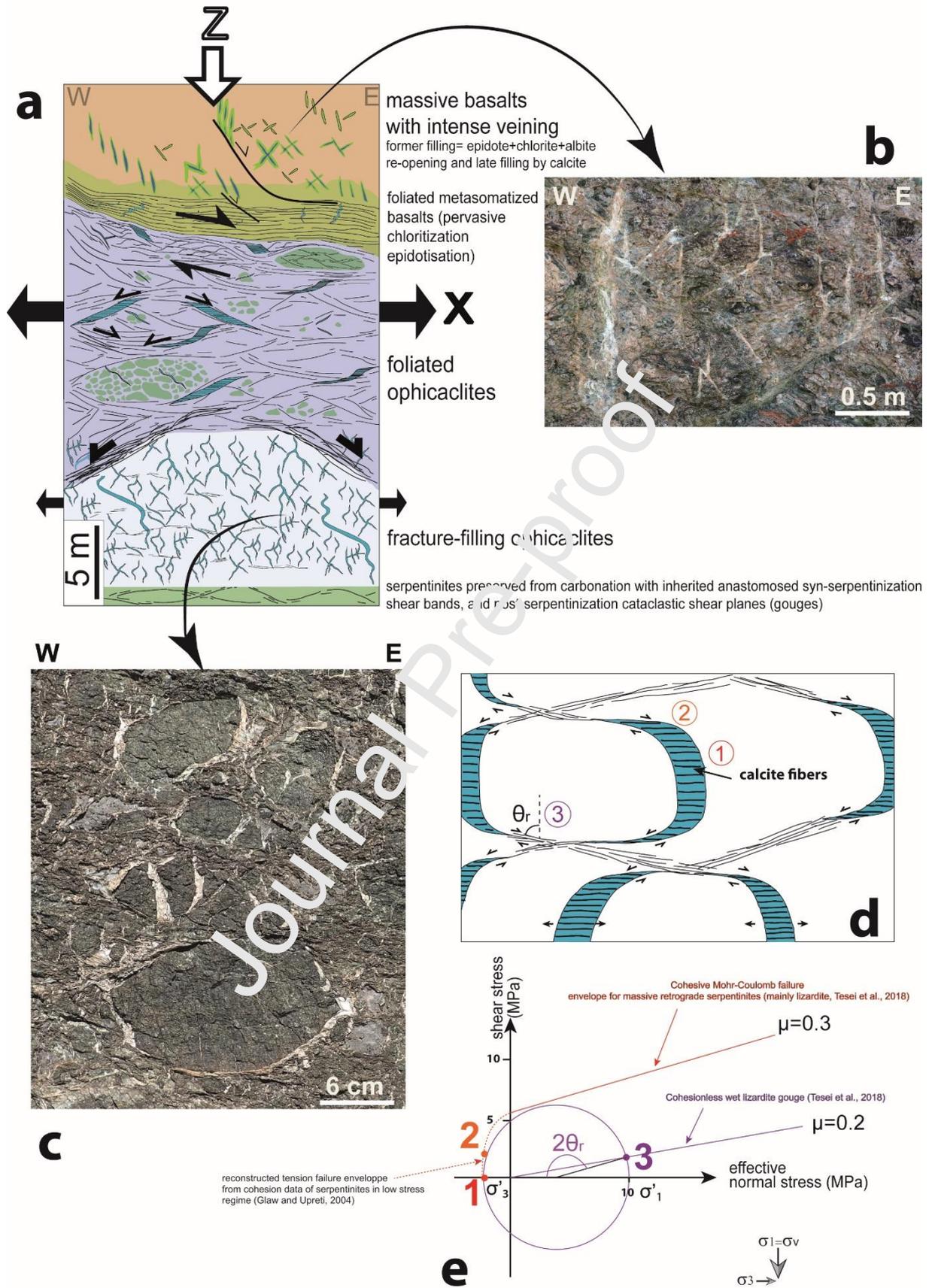
Figure 9. (a) Schematic sketch presenting the strain partitioning across the co-axial decoupling level between basalts and serpentinites from the Falotta outcrop. (b) Picture of

the veined damage zone within the basalt unit with conjugate shear veins and associated en-echelon extensional veins. (c) Crack and shear cockade breccias in the fracture-filling ophicalcites isolating rounded serpentinite clasts. (d) Schematic sketch illustrating calcite stretched crystals ("fibers") in extensional and shear veins associated with pre-existing reactivated shear bands in crack and shear cockade breccias. (e) Mechanical model explaining the formation of crack and shear cockade breccias in ophicalcites. See text for details.

7.3. A fluid-assisted tectono-magmatic model for basalt-serpentinite decoupling

During Jurassic activity, the decoupling basalt-serpentinite interface was at shallow depths under a volcano-sedimentary pile in construction (~2000m below sea level). In the context of ultra-distal rifted margins, slope variations and rapid overloads linked to the construction of volcanic edifices are common features (as in OCC along (ultra)slow-spreading ridges, fig. 1). Therefore, extensional structures and decoupling levels caused through thin-skinned gravity-driven processes are likely and have to be evaluated at Falotta with respect to processes implying thick-skinned extension accommodated by normal faulting within serpentinized mantle rocks.

Two main gravity-driven processes may be distinguished and combined in such context triggering thin-skinned decoupling level (see Brun and Fort, 2011 for a review and references therein): i) the spreading of accumulating overburdens (sediments and/or volcanics) over low-strength rock horizons that accommodate differential loading with lateral flows. Spreading is also identified during the collapse of volcanic edifices on weak basement horizons (e.g. Borgia et al., 1992; Borgia, 1994). Within decoupling level, such a mechanism induces shear regimes and stretching directions fully dependent on the initial geometries of free boundaries. For instance, in the case of a volcanic cone, spreading creates radial grabens with a concentric horizontal stretching (Merle and Borgia, 1996); with non-cylindric geometries of volcanic edifices and lavas flow, variations in stretching direction are expected. Thus, the regular E-W horizontal stretching observed in the decoupling level of Falotta does not favor such a pure spreading mechanism; ii) the gliding of rocks over low-strength slightly-dipping horizons implies dominant simple shear in the decoupling level, which is not in accordance with the co-axial regime highlighted at Falotta. Therefore, the extensional structures associated with the co-axial decoupling interface are unlikely explained by gravity-driven processes and then do not participate to "pure" thin-skinned tectonics.

Accounting for the recognition of high-angle normal faults affecting the serpentinite basement (Epin et al., 2017 and e.g. west of Falotta outcrop, fig. 2c), we propose that the decoupling at the basalt-serpentinite interface occurred in response to basement-involved normal faulting in serpentinized mantle rocks (fig. 10). Such a tectonic pattern and decoupling mechanism are well characterized in association with rheological weak levels (e.g. salt) and are responsible for horsts, grabens and draping structures formation (Maurin, 1985; Vendeville, 1988; Withjack et al., 1990; Nalpas and Brun, 1993; Vendedeville et al., 1995; Withjack and Calloway, 2000; Jackson and Hudec, 2017). However, a constant dip-direction for serpentinite-rooted normal faults (e.g. all normal faults are top-to-the-west in serpentinites) is unable to explain the opposite kinematics of low-angle normal faults and more generally the observed co-axial regime along the decoupling level. For that reason, we propose that during the Jurassic rifting, Falotta was a horst flanked with two active serpentinite-rooted normal faults (fig. 10). The eastern normal fault on the figure 10 is speculative since we have no evidence for it. The scale of the horst structure is thus approximative. However, Jurassic top-to-the-east normal faults have been interpreted in the exhumed Platta domain (Epin et al., 2017; Epin et al., 2019). It is difficult to determine where these normal faults root at depth. They could either branch onto a decoupling level corresponding to the 15% serpentinization rheological interface (Gillard et al., 2019) or onto a level of mafic underplating at the brittle-ductile transition (Manatschal et al., 2011).

This proposed model is fully dependent on the coupling degree between basalts and serpentinites, i.e. the ability of basalts to slip and deformed rather than to be directly cut by fault propagating upward from the major normal fault in the serpentinite basement. The controlling factors of coupling during active normal faulting beneath a weak rheological layer have been studied through analogue modeling by Withjack and Calloway (2000). Decoupling and distributed deformation in the overburden are favored by: (i) a high thickness of viscous decoupling levels; and (ii) a low thickness of the overburden. At Falotta, because basalts are not covered by post-rift sediments and due to Alpine tectonics and glacial erosion, it is difficult to estimate their initial thickness (which is originally highly variable as expected for all volcanic constructs). Therefore, we have no constraints on the thickness ratio between the overburden material and the rheological weak layer; (iii) a high cohesive strength or "ductility" of overburden rocks; here "ductility" refers to the ability of the overburden material to accommodate offset of underlying normal fault by flexure and folding (i.e. drap folding). There are several lines of evidence supporting the fact that the basaltic piles of this

part of the Platta nappe might have accommodated such a flexure during Jurassic rifting. Firstly, the pervasive chloritization of the basalts was likely responsible for an important softening during and shortly after basaltic lavas spread. Secondly, as shown by logs along thicker basaltic piles in the Platta domain (Epin et al., 2019), several sedimentary (e.g. radiolarian cherts) and hyaloclastites horizons are intercalated between basaltic lava flows. At Falotta, the basaltic pile is not homogenous. Rather it presents horizontal layering and anisotropies that are able to accommodate a flexure by flexural slip for example; (iv) a low offset along the normal faults in the basement; reconstructions do not show important offsets (no more than ~300m in the fig. 7 of Epin et al., 2017); (v) a low viscosity of the decoupling layer; high fluid flows are likely responsible for lowering the bulk viscosity of the interface by decreasing the friction of previous serpentinite breccias and softening rocks through carbonation and chloritization. Thus, even though some coupling controls remain unquantifiable, the qualitative evaluation presented here argues for the likelihood of such a normal-fault-induced decoupling level.

The effects of the mafic pile load on the regional normal fault pattern needs to be evaluated. Indeed, if the basement contains ductile layers volcanic piles in rift settings may trigger densification, deflection and capture of normal faults through their own mass (Van Wyck de Vries and Merle, 1997). In the Platta domain it is difficult to recognize individual volcanic edifices, but geological and structural maps indicate that mafic extrusives are abundant especially westward (fig. 2b). Thus, once initiated, basaltic piles might have exerted a spatial control on the distribution of normal faults within serpentinites, enhancing the reactivation of the interface below volcanic flows. Thus, normal faulting would have efficiently controlled the localization of new magma plumbing systems that would have fed in turn the volcanic pile. In that case, it resulted in a positive genetical feedback between normal faulting and magmatic systems. A major result of such an effect of volcanic loading on normal fault pattern distribution may be the spatial coincidence of volcanic piles with underlying basement-involved normal faults controlling the localization of graben and horst structures (fig. 10c).

Finally, the integrated amount of slip along the co-axial decoupling level we depict at Falotta was probably low as it is inferred from the small offsets visible along the low-angle normal faults. However, this does not prevent situations where volcanic piles are located above major normal faults (fig. 10c, left cartoon). In that case, the amount of slip and strain along the

decoupling level would be larger and achieved through mostly non-co-axial regime, a distinct case from what we see at Falotta.

At a larger scale, the decoupling level pointed out at Falotta represents a shallow rheological weak interface. Deeper roughly flat-lying rheological interfaces have been imaged through geophysical methods at the mantle-crust boundary in distal margins (Perez-Guissinye and Reston, 2001; Reston, 2009) or directly in ultramafic rocks in ultra-distal rifted margins or in oceanic settings. There, they would correspond to the peridotite-serpentinized mantle interface (Escartin et al., 2003) or the 15% serpentinization front (Gillard et al., 2019). Hence this shallow decoupling level should be viewed as an important reflector on seismic profiles and likely would help to recognize the interface between serpentinized mantle rocks and the overlying basalts.
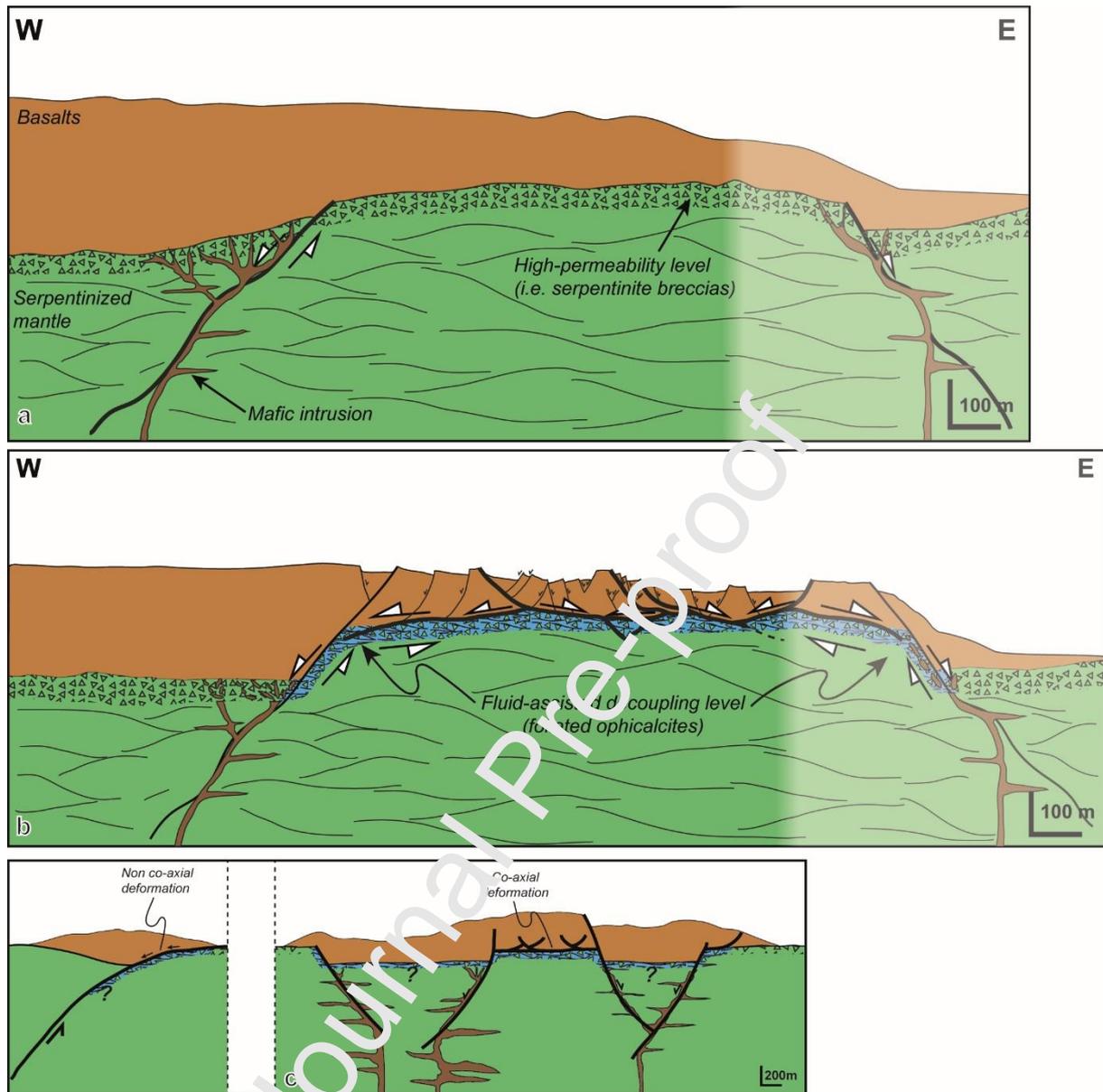
Figure 10. Fluid-assisted tectono-magmatic model explaining the co-axial decoupling observed at the basalt-serpentinite interface at Falotta. The shaded areas on (a) and (b) are putative. (a) Magmatic stage. Basaltic lavas spread over serpentinite breccias and gouges. Magma feeding systems are localized by incipient conjugate normal faulting. (b) Co-axial decoupling at the basalt-serpentinite interface in response to on-going basement-involved normal faulting. Feeder dykes are dismembered and hydrothermal fluids are channelized along the active interface. Greenschist facies metasomatism of basalts and hot carbonation of serpentinite breccias and gouges (ophicalcites) occurred during this stage. (c) Proposed geometry of the Falotta system highlighting the co-axial regime during the Jurassic time

documented here. To the left, a sketch illustrating a distinct non-co-axial deformation related to a major exhumation normal fault.

8. CONCLUSIONS

The basalt-serpentinite interface of a preserved ultra-distal part of a magma-poor rifted margin in the Alpine Tethys realm is well exposed at the Falotta outcrop (Platta nappe). Our study allowed to depict deformation mechanisms and synchronous fluid circulation, which occurred during extensional tectonic processes. Several points have been highlighted in this study:

(1) The foliated nature of the interface between serpentinites and basalts does not correspond to an Alpine contact. Rather it was inherited from Jurassic extensional tectonics during mantle exhumation but after basalt emplacement.

(2) After the deposition of basalts onto the exhumed detachment surface, the interface was reactivated during on-going extensional tectonics as a roughly flat decoupling level showing bulk co-axial deformation.

(3) The deformation at the reactivated interface between basalts and serpentinites was fluid-assisted as shown by the greenschist type alteration of the basalts and late carbonation.

(4) Syn-tectonic fluid circulation allowed to soften the interface with a positive feedback between fluid circulation and extensional deformation.

By inference to what has been highlighted at Falotta, it can be emphasized that, in the Alpine realm the nature of the foliated interface between mafic extrusives and serpentinites does not necessarily correspond to an Alpine contact. Also, in present-day oceanic settings, a roughly flat tectonic contact between mafic extrusives and serpentinites is not necessarily indicative of faulting activity cutting through a former mafic crust (i.e. rafted block) but may signify syn-magmatic deformation once mafic extrusives have spread on serpentinites after mantle exhumation at the seafloor. The existence of this third type of relation at the interface between basalts and serpentinized mantle rocks (i.e. after rafted blocks and nonconformity shown in fig. 1) should be kept in mind when examining (i) geophysical images in present-day oceanic domains (e.g., fig. 1a-c) and (ii) onland rock exposures that underwent a strong orogenic overprint, like in blueschist facies units.

ACKNOWLEDGMENTS

REFERENCES

Berger, A., Herwegh, M., 2019. Cockade structures as a paleo-earthquake proxy in upper crustal hydrothermal systems. Nature Scientific Reports 9, 1-9. doi:10.1038/s41598-019-45488-2

Bernoulli, D., Weissert, H.J., 1985. Sedimentary fabrics in Alpine ophicalcites, South Pennine Arosa zone, Switzerland. Geology 13, 755–758.

Blackman, D.K., et al., 2011. Drilling constraints on lithospheric accretion and evolution at Atlantis Massif, Mid-Atlantic Ridge 30°N. J. Geophys. Res. 116, 1–25. doi:10.1029/2010JB007931

Boillot, G., Beslier, M.O., Krawczyk, C.M., Rappin, D., Reston, T.J., 1995. The formation of passive margins: constraints from the crustal structure and segmentation of the deep Galicia margin, Spain. Geol. Soc. London, Spec. Publ. 71–91

Boillot, G., Recq, M., Winterer, E.L., Meyer, A.W., Applegate, J., Baltuck, M., Bergen, J.A., Comas, M.C., Davies, T.A., Dunham, K., Evans, C.A., Girardeau, J., Goldberg, G., Haggerty, J., Jansa, L.F., Jonhson, J.A., Kasahara, J., Loreau, J.P., Luna-Sierra, E., Moullade, M., Ogg, J., Thurow, J., Williamson, M., 1987. Tectonic denudation of the upper mantle along passive margins: a model based on drilling results (ODP leg 103 , western Galicia margin, Spain). Tectonophysics 132, 335–342.

Bonatti, E., Emiliani, C., Ferrara, G., Honnorez, J., Rydell, H., 1974. Ultramafic-carbonate breccias from the equatorial Mid Atlantic Ridge. Mar. Geol. 16, 83–102. https://doi.org/doi:10.1016/0025-3227(74)90057-7

Bons, P.D., Elburg, M.A., Gomez-Rivas, E., 2012. A review of the formation of tectonic veins and their microstructures. J. Struct. Geol. 43, 33–62. doi:10.1016/j.jsg.2012.07.005

Borgia, A., 1994. Dynamic basis of volcanic spreading. J. Geophys. Res. 99, 17791–17804.

Borgia, A., Ferrari, L., Pasquarè, G., 1992. Importance of gravitational spreading in the tectonic and volcanic evolution of Mount Etna. Nature 357, 231–235.

Brun, J.P., Fort, X., 2011. Salt tectonics at passive margins: Geology versus models. Mar. Pet. Geol. 28, 1123–1145. doi:10.1016/j.marpetgeo.2011.03.004

Canales, J.P., Tucholke, B.E., Collins, J.A., 2004. Seismic reflection imaging of an oceanic

detachment fault: Atlantis megamullion (Mid-Atlantic Ridge, 30°10′N). Earth Planet. Sci. Lett. 222, 543–560. https://doi.org/doi:10.1016/j.epsl.2004.02.023

Cann, J.R., Blackman, D.K., Smith, D.K., McAllister, E., Janssen, B., Mello, S., Avgerinos, E., Pascoe, A.R., Escartin, J., 1997. Corrugated slip surfaces formed at ridge–transform intersections on the Mid-Atlantic Ridge. Nature 385, 329–332. doi:10.1038/385329a0

Coltat, R., Boulvais, P., Branquet, Y., Collot, J., Epin, M.E., Manatschal, G., 2019a. Syntectonic carbonation during synmagmatic mantle exhumation at an ocean-continent transition. Geology 47, 183–186. doi:10.1130/G45530.1

Coltat, R., Branquet, Y., Gautier, P., Campos Rodriguez, H., Poujol, M., Pelleter, E., McClenaghan, S., Manatschal, G., Boulvais, P., 2019b. Unravelling the root zone of ultramafic-hosted black smokers-like hydrothermalism from an Alpine analog. Terra Nov. 31, 549–561. doi:10.1111/ter.12427

Decarlis, A., Gillard, M., Tribuzio, R., Epin, M.E., Manatschal, G., 2018. Breaking up continents at magma-poor rifted margins: a seismic vs. outcrop perspective. J. Geol. Soc. London. 175.

Desmurs, L., Manatschal, G., Bernoulli, D., 2001. The Steinmann Trinity revisited: mantle exhumation and magmatism along an ocean-continent transition: the Platta nappe, eastern Switzerland. Geol. Soc. Am. Spec. Pap. 167, 235–266.

Desmurs, L., Müntener, O., Manatschal, G., 2002. Onset of magmatic accretion within a magma-poor rifted margin: a case study from the Platta ocean-continent transition, eastern Switzerland. Contrib. to Mineral. Petrol. 144, 365–382. doi:10.1007/s00410-002-0403-4

Dietrich, V., 1969. Die Ophiolithe des Oberhalbsteins (Graubünden) und das Ophiolithmaterial der ostschweizerischen Molasseablagerungen, ein petrographischer Vergleich, 187p.

Dietrich, V., 1970. Die Stratigraphie der Platta-Decke: facielle Zusammenhänge zwischen Oberpenninikum und Unterostalpin. Eclogae Geol. Helv. 63, 631–671.

Dietrich, V., Vuagnat, V., Bertrand, M., 1974. Alpine metamorphism of mafic rocks. Schweizerische Mineral. und Petrogr. Mitteilungen 54, 291–332.

Epin, M., Manatschal, G., Amannn, M., 2017. Defining diagnostic criteria to describe the role of rift inheritance in collisional orogens: the case of the Err-Platta nappes (Switzerland). Swiss J. Geosci. 110, 419–438. doi:10.1007/s00015-017-0271-6

Epin, M.E., Manatschal, G., Amman, M., Ribes, C., Clausse, A., Guffon, T., Lescanne, M., 2019. Polyphase tectono-magmatic evolution during mantle exhumation in an ultra-distal, magma-poor rift domain: example of the fossil Platta ophiolite, SE Switzerland. Int. J. Earth Sci. 108, 2443–

2467. doi:10.1007/s00531-019-01772-0

Escartın, J., Mével, C., Macleod, C.J., Mccaig, A.M., 2003. Constraints on deformation conditions and the origin of oceanic detachments: The Mid-Atlantic Ridge core complex at 15°45'N. Geochemistry, Geophys. Geosystems 4, 1–37. doi:10.1029/2002GC000472

Ferreiro Mählmann, R., 2001. Correlation of very low grade data to calibrate a thermal maturity model in a nappe tectonic setting, a case study from the Alps. Tectonophysics 334, 1–33.

Ferreiro Mählmann, R., 1995. Das Diagenese-Metamorphose-Muster von Vitrinitreflexion und Illit-" Kristallinität" in Mittelbünden und im Oberhalbstein, Teil 1: Bezüge zur Stockwerktektonik. Schweizerische Mineral. und Petrogr. Mitteilungen 75, 85–122. https://doi.org/doi:10.5169/seals-57145 Nutzungsbedingungen

Froitzheim, N., Eberli, G.P., 1990. Extensional detachment faulting in the evolution of a Tethys passive continental margin, Eastern Alps, Switzerland. Geol. Soc. Am. Bull. 102, 1297–1308.

Froitzheim, N., Manatschal, G., 1996. Kinematics of Jurassic rifting, mantle exhumation, and passive-margin formation in the Austroalpine and Penninic nappes (eastern Switzerland). Geol. Soc. Am. Bull. 108, 1120–1133.

Froitzheim, N., Schmid, S.M., Conti, P., 1994. Repeated change from crustal shortening to orogen-parallel extension in the Austroalpine units of Graubünden Graubünden. Eclogae Geol. Helv. 87, 559–612.

Gillard, M., Autin, J., Manatschal, G., 2016a. Fault systems at hyper-extended rifted margins and embryonic oceanic crust: Structural style, evolution and relation to magma. Mar. Pet. Geol. 76, 51–67. doi:10.1016/j.marpetgeo.2016.05.013

Gillard, M., Manatschal, G., Autin, J., 2016b. How can asymmetric detachment faults generate symmetric Ocean Continent Transitions? Terra Nov. 28, 27–34. doi:10.1111/ter.12183

Gillard, M., Sauter, D., Tugend, J., Tomasi, S., Epin, M., Manatschal, G., 2017. Birth of an oceanic spreading center at a magma-poor rift system. Nat. Sci. Reports 7, 1–6. doi:10.1038/s41598-017-15522-2

Gillard, M., Tugend, J., Müntener, O., Manatschal, G., Karner, G.D., Autin, J., Sauter, D., Figueredo, P.H., Ulrich, M., 2019. The role of serpentinization and magmatism in the formation of decoupling interfaces at magma-poor rifted margins. Earth-Science Rev. 196, 102882. doi:10.1016/j.earscirev.2019.102882

Glawe, U., Upreti, B.N., 2004. Better understanding the strengths of serpentinite bimrock and homogeneous serpentinite. Felsbau 22, 53–60.

Handy, M.R., 1996. The transition from passive to active margin tectonics: a case study from the zone of Samedan (eastern Switzerland). Geol. Rundschau 85, 832–851. doi:10.1007/BF02440114

Handy, M.R., Herwegh, M., Kamber, B.S., Tietz, R., Villa, I.M., 1996. Geochronologic, petrologic and kinematic constraints on the evolution of the Err-Platta boundary, part of a fossil continent-ocean suture in the Alps (eastern Switzerland). Schweizerische Mineral. und Petrogr. Mitteilungen. doi:10.7892/boris.73902

Hopper, J.R., Funck, T., Tucholke, B.E., Larsen, H.C., Holbrook, W.S., Louden, K.E., Shillington, D., Lau, H., 2004. Continental breakup and the onset of ultraslow seafloor spreading off Flemish Cap on the Newfoundland rifted margin. Geology 32, 93–96. doi:10.1130/G19694.1

Ildefonse, B., Blackman, D.K., John, B.E., Ohara, Y., Miller, D.J., MacLeod, C.J., Party, I.O.D.P.E. 304/305 S., 2007. Oceanic core complexes and crustal accretion at slow-spreading ridges. Geology 35, 623–626. doi:10.1130/G23531A.1

Jackson, M.P.A., Hudec, M.R., 2017. Salt tectonics: Principles and practice.

Karson, J.A., Früh-Green, G.L., Kelley, D.S., Williams, E.A., Yoerger, D.R., Jakuba, M., 2006. Detachment shear zone of the Atlantis Massif core complex, Mid-Atlantic Ridge, 30°N. Geochemistry, Geophys. Geosystems 7 1–29. doi:10.1029/2005GC001109

Karson, J.A., Winters, A.T., 1992. Along-axis variations in tectonic extension and accommodation zones in the MARK Area, Mid-Atlantic Ridge 23°N latitude. Geol. Soc. London, Spec. Publ. 60, 107–116. doi:10.1144/GSL.SP.1992.060.01.06

Lagabrielle, Y., Bideau, D., Cannat, M., Karson, J.A., Mével, C., 1998. Ultramafic-Mafic Plutonic Rock Suites Exposed Along the Mid-Atlantic Ridge (10 N-30 N) Symmetrical-Asymmetrical Distribution and Implications for Seafloor Spreading Processes. Geophys. Monogr. Geophys. UNION 106, 153–176.

Lagabrielle, Y., Cannat, M., 1990. Alpine Jurassic ophiolites resemble the modern central Atlantic basement. Geology 18, 319–322.

Lagabrielle, Y., Vitale, A., Ildefonse, B., 2015. Fossil oceanic core complexes recognized in the blueschist metaophiolites of Western Alps and Corsica. Earth Sci. Rev. 141, 1–26. doi:10.1016/j.earscirev.2014.11.004

Lemoine, M., Tricart, P., Boillot, G., 1987. Ultramafic and gabbroic ocean floor of the Ligurian Tethys (Alps, Corsica, Apennines): In search of a genetic model. Geology 15, 622–625.

Macleod, C.J., Searle, R.C., Murton, B.J., Casey, J.F., Mallows, C., Unsworth, S.C., Achenbach, K.L., Harris, M., 2009. Life cycle of oceanic core complexes. Earth Planet. Sci. Lett. 287, 333–344.

doi:10.1016/j.epsl.2009.08.016

Manatschal, G., 1995. Jurassic rifting and formation of a passive continental margin (Platta and Err nappes, Eastern Switzerland): geometry, kinematics and geochemestry of fault rocks and a comparision with the Galicia margin. 269p.

Manatschal, G., Engström, A., Desmurs, L., Schaltegger, U., Cosca, M., Müntener, O., Bernoulli, D., 2006. What is the tectono-metamorphic evolution of continental break-up: The example of the Tasna Ocean-Continent Transition. J. Struct. Geol. 28, 1849–1869. doi:10.1016/j.jsg.2006.07.014

Manatschal, G., Nievergelt, P., 1997. A continent-Ocean transition recorded in the Err and Platta nappes (Eastern Switzerland). Eclogae Geol. Helv. 90, 3–27.

Manatschal, G., Sauter, D., Marie, A., Masini, E., Mohn, G., Lagabrielle, Y., 2011. The Chenaillet Ophiolite in the French/Italian Alps : An ancient analogue for an Oceanic Core Complex ? LITHOS 124, 169–184. doi:10.1016/j.lithos.2010.10.017

Maurin, J.-C., 1995. Drapage et décollement des séries jurassiques sur la faille de détachement majeure du rift rhénan sud : implications sur la géométrie des dépôts syn-rifts oligocènes. Comptes rendus l'Académie des Sci. Série I. Sci. la terre des planètes 321, 1025–1032.

Merle, O., Borgia, A., 1996. Scaled experiments of volcanic spreading. J. Geophys. Res. 101, 13805–13817.

Mohn, G., Manatschal, G., Masini, E., Müntener, O., 2011. Rift-related inheritance in orogens: a case study from the Austroalpine nappes in Central Alps (SE-Switzerland and N-Italy). Int. Geol. Rev. 100, 937–961. doi:10.1007/s00531-010-0630-2

Müntener, O., Manatschal, G., Desmurs, L., Pettke, T., 2010. Plagioclase Peridotites in Ocean-Continent Transitions: Refertilized Mantle Domains Generated by Melt Stagnation in the Shallow Mantle Lithosphere. J. Petrol. 51, 255–294. doi:10.1093/petrology/egp087

Nalpas, T., Brun, J.P., 1993. Salt flow and diapirism related to extension at crustal scale. Tectonophysics 228, 349–362. doi:10.1016/0040-1951(93)90348-N

Pérez-Gussinyé, M., Reston, T.J., 2001. Rheological evolution during extension at nonvolcanic rifted margins: Onset of serpentinization and development of detachments leading to continental breakup. J. Geophys. Res. 106, 3961–3975.

Picazo, S., Manatschal, G., Cannat, M., Andréani, M., 2013. Deformation associated to exhumation of serpentinized mantle rocks in a fossil Ocean Continent Transition: The Totalp unit in SE Switzerland. LITHOS 175–176, 255–271. doi:10.1016/j.lithos.2013.05.010

Picazo, S., Müntener, O., Manatschal, G., Bauville, A., Karner, G., Johnson, C., 2016. Mapping the nature of mantle domains in Western and Central Europe based on clinopyroxene and spinel chemistry: Evidence for mantle modification during an extensional cycle. Lithos 266–267, 233–263. doi:10.1016/j.lithos.2016.08.029

Principi, G., Bortolotti, V., Chiari, M., Cortesogno, L., Gaggero, L., Marcucci, M., Saccani, E., Treves, B., 2004. The pre-orogenic volcano-sedimentary covers of the Western Tethys Oceanic basin: A review. Ofioliti 29, 177–211. doi:10.4454/ofioliti.v29i2.213

Reston, T.J., 2009. The structure, evolution and symmetry of the magma-poor rifted margins of the North and Central Atlantic: A synthesis. Tectonophysics 468, 6–27. doi:10.1016/j.tecto.2008.09.002

Ribes, C., Manatschal, G., Ghienne, J.F., Karner, G.D., Johnson, C.A., Figueredo, P.H., Incerpi, N., Epin, M.E., 2019. The syn-rift stratigraphic record across a fossil hyper-extended rifted margin: the example of the northwestern Adriatic margin exposed in the Central Alps. Int. J. Earth Sci. 108, 2071–2095. doi:10.1007/s00531-019-01750-6

Richardson, C.J., Cann, J.R., Richards, H.G., Cowan, J.G., 1987. Metal-depleted root zones of the Troodos ore-forming hydrothermal systems, Cyprus. Earth Planet. Sci. Lett. 84, 243–253.

Sauter, D., Cannat, M., Rouméjon, S., Andreani, M., Birot, D., Bronner, A., Brunelli, D., Carlut, J., Delacour, A., Guyader, V., MacLeod, C.J., Manatschal, G., Mendel, V., Ménez, B., Pasini, V., Ruellan, E., Searle, R., 2013. Continuous exhumation of mantle-derived rocks at the Southwest Indian Ridge for 11 million years. Nat. Geosci. 6, 314–320. doi:10.1038/ngeo1771

Schaltegger, U., Desmurs, L., Manatschal, G., Müntener, O., Meier, M., Frank, M., Bernoulli, D., 2002. The transition from rifting to sea-floor spreading within a magma-poor rifted margin: field and isotopic constraints. Terra Nov. 14, 156–162.

Schmid, S.M., Pfiffner, A., Froitzheim, N., Schönborn, G., Kissling, E., 1996. Geophysical-geological transect and tectonic evolution of the Swiss-Italian Alps. Tectonics 15, 1036–1064.

Tesei, T., Harbord, C.W.A., De Paola, N., Collettini, C., Viti, C., 2018. Friction of Mineralogically Controlled Serpentinites and Implications for Fault Weakness. J. Geophys. Res. Solid Earth 123, 6976–6991. doi:10.1029/2018JB016058

Treves, B., Harper, G.D., 1994. Exposure of serpentinites on the ocean floor: sequence of faulting and hydrofracturing in the Northern Apennine ophicalcites. Ofioliti 19, 435–466.

Tricart, P., Lemoine, M., 1983. Serpentinite oceanic botton in South Queyras ophiolites (French Western Alps): record of the incipient oceanic opening of the Mesozoic Ligurian Tethys. Eclogae Geol. Helv. 76, 611–629.

Trümpy, R., 1975. Penninic-Austroalpine boundary in the Swiss Alps: a presumed former continental margin and its problems. Am. J. Sci. 275, 209–238.

Tucholke, B.E., Fujioka, K., Ishihara, T., Hirth, G., Kinoshita, M., 2001. Submersible study of an oceanic megamullion in the central North Atlantic. J. Geophys. Res. Solid Earth 106, 16145–16161. doi:10.1029/2001JB000373

Tucholke, E., Lin, J., Kleinrock, C., 1998. Megamullions and mullion structure defining oceanic metamorphic core complexes on the Mid-Atlantic Ridge. J. Geophys. Res. 103, 9857–9866.

van Wyk de Vries, B., Merle, O., 1996. The effect of volcanic constructs on rift fault patterns. Geology 24, 643–646.

Vendeville, B.C., 1988. Modèles expérimentaux de fracturation de la couverture contrôlée par des failles normales dans le socle. Comptes rendus l'Académie des Sci. Série 2, Mécanique, Phys. Chim. Sci. l'univers, Sci. la Terre 307, 1013–1018.

Vendeville, B.C., Ge, H., Jackson, M.P.A., 1995. Scale models of salt tectonics during basement-involved extension. Pet. Geosci. 1, 179–183. https://doi.org/doi:10.1144/petgeo.1.2.179

Weissert, H.J., Bernoulli, D., 1984. Oxygen isotope composition of calcite in Alpine ophicarbonates: a hydrothermal or Alpine metamorphic signal? Eclogae Geol. Helv. 77, 29–43.

Weissert, H.J., Bernoulli, D., 1985. A transform margin in the Mesozoic Tethys: evidence from the Swiss Alps. Geol. Rundschau 74, 665–679.

Welford, J.K., Smith, J.A., Hall, J., Deemer, S., Srivastava, S.P., Sibuet, J.-C., 2010. Structure and rifting evolution of the northern Newfoundland Basin from Erable multichannel seismic reflection profiles across the southeastern margin of Flemish Cap. Geophys. J. Int. 180, 976–998. doi:10.1111/j.1365-246X.2009.04477.x

Withjack, M.O., Callaway, S., 2000. Active normal faulting beneath a salt layer: An experimental study of deformation patterns in the cover sequence. Am. Assoc. Pet. Geol. Bull. 84, 627–651. doi:10.1306/c9ebce73-1735-11d7-8645000102c1865d

Withjack, M.O., Olson, J., Peterson, E., 1990. Experimental Models of Extensional Forced Folds. Am. Assoc. Pet. Geol. Bull. 74, 1038–1054. doi:10.1306/0C9B23FD-1710-11D7-8645000102C1865D

Credit Author statement

Declaration of interests

☒ The authors declare that they have no known competing financial interests or personal relationships that could have appeared to influence the work reported in this paper.

☐The authors declare the following financial interests/personal relationships which may be considered as potential competing interests:

HIGHLIGHTS

- Deformation at the basalt-serpentinite interface occurred under oceanic extension

- The interface acted as a decoupling level with bulk co-axial deformation

- The contact was not reactivated during Alpine overprint

- Fluid-assisted deformation led to carbonation of the basalts and serpentinites

- A third type of oceanic basalt-serpentinite interface is defined